Applied Materials Today 18 (2020) 100509

Contents lists available at ScienceDirect

Applied Materials Today

journal homepage: www.elsevier.com/locate/apmt

MXenes—A new class of 2D layered materials: Synthesis, properties, applications as supercapacitor electrode and beyond

Sandhya Venkateshalu, Andrews Nirmala Grace*

Centre for Nanotechnology Research, Vellore Institute of Technology (VIT), Vellore 632014 Tamil Nadu, India

ARTICLE INFO

Article history:
Received 8 August 2019
Received in revised form 8 November 2019
Accepted 13 November 2019

Keywords:
MXene
Supercapacitor
Energy storage
2D materials

ABSTRACT

Since the discovery of Ti_3C_2 MXene in 2011, continuous research has been progressed in developing new MAX phases and extracting MXenes from them. The surface terminations such as -O, -OH, -F groups present on the MXene influence their properties to a wide extent. By controlling the inter-layer spacing between the MXene sheets and the number of MXene layers, their properties can be tuned greatly. Their 2D structure with unique compositions has helped them obtain properties that are useful in various fields of applications such as batteries, supercapacitors, photo and electrocatalysts, bio-sensors, gas-sensors, water purification, water splitting, lubricants, electronics, electromagnetic interference shielding and so on. This review focuses on the synthesis, properties and applications of MXenes outlining the current challenges and scope for future research.

Contents

1. Introduction

Batteries the widely used storage systems face the problem of low power density while exhibiting excellent energy density. Capacitors exhibit excellent power density but poor energy density. Supercapacitors are currently the widely researched storage systems which exhibit the properties of both batteries as well as capacitors. The performance of supercapacitor can be enhanced by changing the electrode materials [1,2]. Based on the type of electrode materials used, the supercapacitors are further classified as electrochemical double layer capacitors (EDLC) and pseudocapacitors [3]. EDLC based supercapacitors are formed with the use of carbonaceous materials as its electrode [4]. EDLC based superca-

* Corresponding author.
E-mail address: anirmalagrace@vit.ac.in (A.N. Grace).

https://doi.org/10.1016/j.apmt.2019.100509
2352-9407/

pacitors store charges based on non-faradaic reactions whereas pseudocapacitors store charges based on Faradaic reactions [5]. Conducting polymers, metal oxides, metal sulfides, metal nitrides and tellurides constitute the electrode materials for pseudocapacitors. Each of these materials has its own advantages and disadvantages compared to each other [6]. In the quest for developing advanced electrode materials for supercapacitors, various research works have been carried out.

Two dimensional nanomaterials are those that have two dimensions outside the nanoscale range. The quest for developing 2D nanostructured materials increased after the discovery of the 'wonder material' Graphene by Novoselov and Geim [7]. With the excellent optical, electrical, thermal and mechanical properties exhibited by graphene, it has found outstanding applications in almost every field of research [8,9]. Due to the unique physical and chemical properties exhibited by 2D material graphene, various other 2D materials such as hexagonal boron nitride (hBN) [10], transition metal dichacolgenides (TMDs) [11], metal–organic frameworks (MOFs) [12], Metal oxides [13], germanane, silicene [13] and phosphorene [14] gained much attention. Recently a new group of 2D materials known as MXenes discovered by Gogotsi and Barsoum in 2011 have attracted researchers due to its impeccable properties [15]. MXenes belong to the family of transition metal carbides, nitrides and carbonitrides. They are formed by the selective etching of 'A' layers from their MAX phases with general formula $M_{n+1}AX_n$ where, n = 1, 2 or 3, M is the early transition metal (Ti, V, Cr, Mn, Zr, Nb, Mo or Ta), A is group 13 or 14 element (Al, Ga, In, Si, Ge, As, Sn or Pb), and X is either or both carbon or nitrogen [16]. These MAX phases are layered hexagonal structures with a space group $D_{6h}{}^4$-$P6_3/mmc$ and with two formula units per cell. Closely packed M–layers are interleaved with layers of group A element and X atoms fill up the octahedral sites between the former [17]. The M—X bond exhibit strong covalent/metallic/ionic character, whereas the bond between M—A is metallic in nature. In comparison with other layered materials such as graphene and TMD's [7,11], where weak van der Waals interactions hold the layers together, the bonds in the MAX phases are too strong to be broken. However, the M—A bonds are slightly weaker when compared to the M—X bond and using this phenomenon of relative bond energies, the A atoms can be selectively etched from the MAX phases by strong acids or molten salts without disrupting the M—X bonds [18]. The 2D material formed after the selective etching of A layers from its MAX phase was named MXene in order to highlight its graphene-like morphology. This so formed MXene has a formula $M_{n+1}X_nT_x$ where, T_x refers to the surface terminated functional groups (-O, -OH, -F) attached on to the M atoms after the etching procedure. According to Barsoum, using the vast number of combinational possibilities from the three elements of the MAX phase, more than 60 MAX phases have been produced so far, but only a few MXenes from those are reported till date [19]. This has opened a challenge among researchers in exploring new MXenes. Depending on the value of n, three phases have known to exist such as 211, 312 and 413 phases (M_2AX, M_3AX_2 and M_4AX_3) as shown in Fig. 1 [20]. Among the three phases, a majority are the 211 phases. Many more MXenes are expected to be produced from their MAX phases in future thus providing a lot of scope in this field of research.

MXenes have found applications in every possible field with its 2D structure and unique properties. MXenes have found wide applications as catalysts for oxygen reduction reaction (ORR) [21,22], oxygen evolution reaction (OER) [23,24], CO oxidation [25], dehydrogenation of hydrogen storage materials [26,27], hydrogen evolution reactions [28,29]. They have also found their applications in sensor technology as electrochemical biosensors [30], gas sensors [31], detection of macromolecules and cells [32] etc. One of the major applications of MXenes is in energy storage devices [33]. MXenes have found its potential as electrodes for Li-ion batteries, Na- ion batteries and supercapacitors [34–37]. Due to the surface terminated functional groups and the layered structures of MXenes, they are seen to provide improved supercapacitive performance compared to other electrode materials. By tuning the inter-layer distances of MXenes, the supercapacitance can also be varied.

With this view, this review article summarizes the current trends in the synthesis of MXenes and outlines its experimental and theoretical challenges. The current progress in MXene research, their properties and potential applications of these exciting 2D materials as supercapacitor electrodes are also well discussed. Although many review articles are found on MXenes, much details on the synthesis of Nitride based MXenes and particularly the etching procedures are not found. Such processes will be detailed and discussed.

2. Synthesis

In general, a MAX phase is initially formed by mixing the elemental powders of M, A and X in particular atomic ratios and heating them to high temperatures. The ball milled samples are usually hot pressed or cold pressed to enable densification and to reduce the amount of structural flaws, such as microvoids and cracks in the material. Pressure applied during the pressing is used to influence the preferred orientation of grain growth. Pressureless sintering is done by just heating the MAX powders to certain temperature. Li et al. reported that Ti_3C_2 obtained by pressureless sintering of Ti_3AlC_2 was highly oriented compared to that obtained from hot-pressed Ti_3AlC_2 [38]. Once the MAX phase is formed, the A element will be etched away to form the MXene. As a result of this, the dense MAX powders will be converted to stacked layers that are loosely packed forming the Multi-layered (ML) MXenes. These ML-MXenes will be further subjected to exfoliation, thereby producing few-layered MXenes. The confirmation regarding the conversion of MAX phase to MXene can be done through X-ray diffraction (XRD) and energy-dispersive spectroscopy (EDS). If there is complete conversion of MAX to MXene then the XRD pattern will contain only *(000 l)* peaks (indicating the loss of order in non-basal directions) and all other peaks will be weak or absent. The *(000 l)* peaks will be broad and downshifted to lower angles indicating an increase in the c lattice parameter. The ratio of A:M will be calculated through EDS; if this ratio is negligible then it indicates complete conversion. The XRD pattern of V_2CT_x MXene is shown in Fig. 2d. It could be seen that only peaks pertaining to *(000 l)* is present in the pattern for V_2CT_x MXene [39].

2.1. Etchants

Etchants are required to break the strong chemical bonds existing between the elements A and M in the MAX phase, thus enabling exfoliation of the material. The etching for most of the carbide based MAX powder is simply done by treating it with an aqueous solution of HF, with a specific concentration and for a particular amount of time. The HF treated MAX powders are subjected to centrifugation followed by washing with DI water until the pH reaches a value between 4 and 6. The solution is then filtered to obtain MXene, the accordion-like structure similar to exfoliated graphite [40]. The layered structures are further subjected to ultrasonication to obtain delaminated structures. This schematic is shown in Fig. 3.

Such treatment leaves surface terminated functional groups onto the surface of the metal and this is described by the following equations [42]:

$$M_{n+1}AX_n + 3HF \rightarrow AF_3 + 3/2H_2 + M_{n+1}X_n \quad (1)$$

$$M_{n+1}X_n + 2H_2O \rightarrow M_{n+1}X_n(OH)_2 + H_2 \quad (2)$$

$$M_{n+1}X_n + 2HF \rightarrow M_{n+1}X_nF_2 + H_2 \quad (3)$$

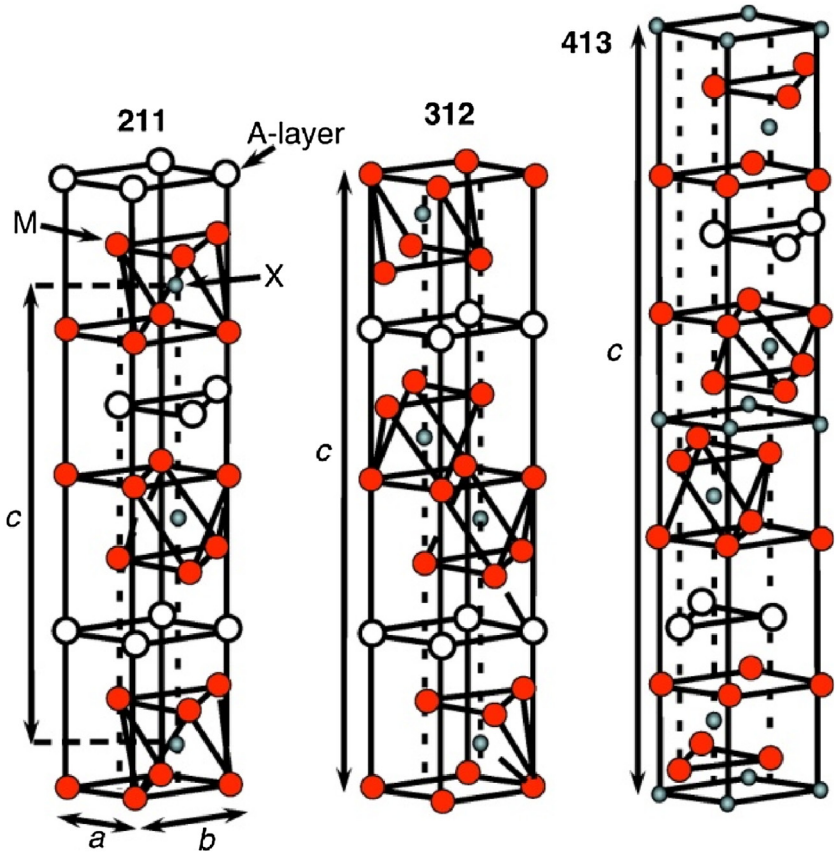

Fig. 1. MAX-phase unit cell structures of 211 (n = 1), 312 (n = 2) and 413 (n = 3).Reproduced with permission from [20] copyright 2016, Elsevier Ltd.

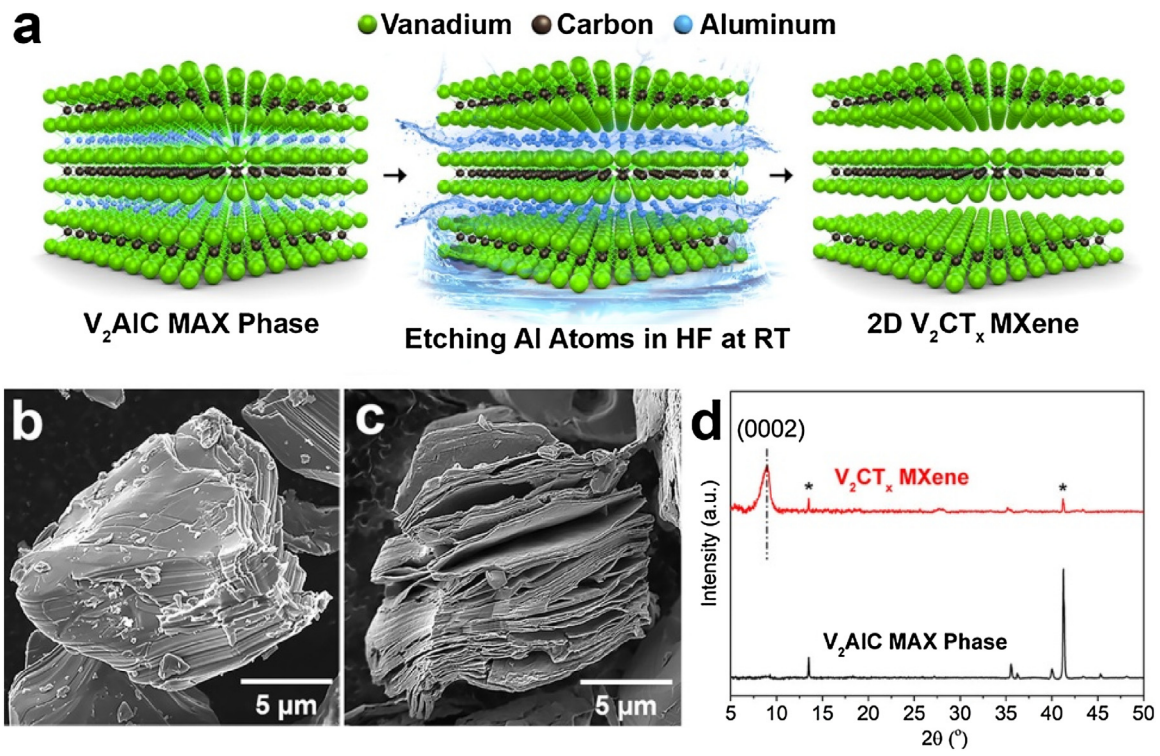

Fig. 2. (a) Schematic illustration of the selective etching process used to synthesize V_2CT_x MXene from V_2AlC MAX phase. (b) SEM image of V_2AlC MAX phase particle. (c) SEM image of V_2AlC treated with 50 % HF for 92 h at room temperature. (d) XRD patterns of V_2AlC before and after HF treatment (V_2CTx MXene). Asterisk (*) denotes the remaining MAX phase residual in the etched powder. Reproduced with permission from [39] copyright 2017, American Chemical Society.

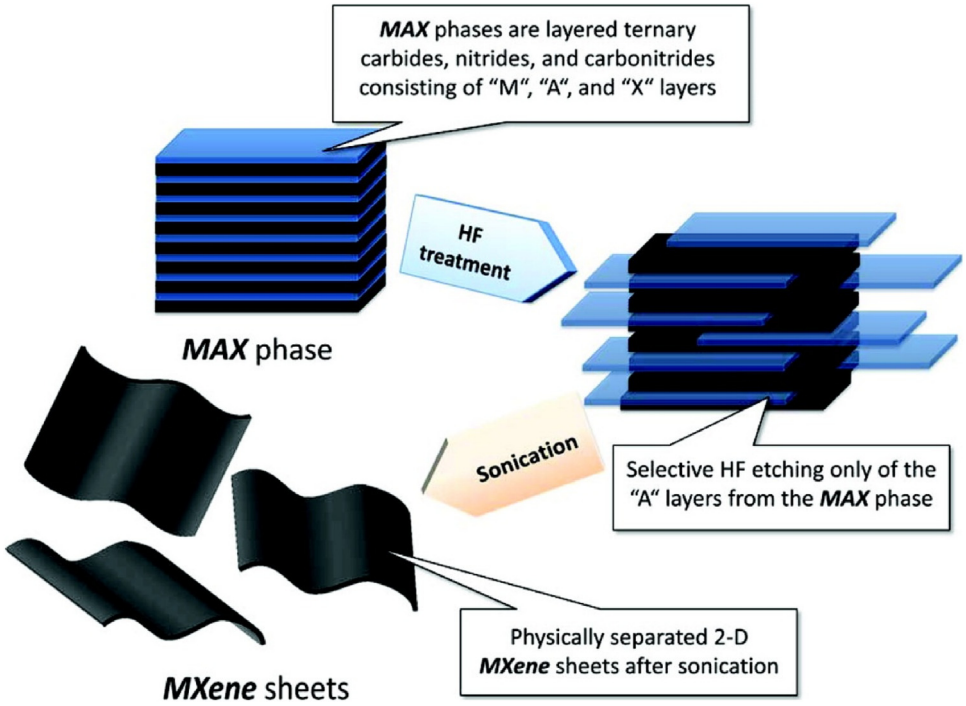

Fig. 3. Schematic for the exfoliation process of MAX phases and formation of MXenes. Reproduced with permission from [41] copyright 2012, American Chemical Society.

Eq. (1) represents the formation of $M_{n+1}X_n$ phase from its MAX phase. Eq.s (2) and (3) represent the surface functionalization of the $M_{n+1}Xn$ phase due to the electrophilic nature of the metal with elements such as OH and F during the etching process. The packed layers are known as multi-layered MXenes and if the layers are less than 5, they are referred as few layered MXene. To obtain these few-layered MXenes, sonication was carried out by intercalating various intercalating agents [18]. By reducing the size of MAX phases by ball milling, the time and concentrations of HF can be reduced [43]. The bond energies of M—A also play a role in deciding the required concentration and time duration of HF [44].

Mohamed Alhabeb et al. reported a detailed work done on the effect of different etchants and delamination methods in the formation of $Ti_3C_2T_x$ [45]. The concentration of the HF acid and the reaction times were all varied and a study was reported on this. It was shown that a 5 wt% HF was able to etch aluminum out of the Ti_3AlC_2 but the accordion-like morphology was observed only for ≥10 wt% HF solutions. The SEM images obtained for V_2AlC treated with 50 wt% HF for 92 h at RT is shown in Fig. 2c. The sheets are clearly visible here for increased reaction time and concentration [39]. Several reports are found on the use of in situ HF formed when an acid-fluoride salt was used as an etchant. Acids (HCl, H_2SO_4) and fluoride salts (NH_4HF_2, KHF_2, $NaHF_2$) were mixed in right proportions to form the etching agents [46–48]. Liu et al. reported an extensive work on the role of different fluoride salts such as LiF, NaF, KF and NH_4F in HCl as etchants for Ti_3AlC_2 and Ti_2AlC [48]. In the work reported by Halim et al., it was seen that when NH_4HF_2 was used as the etching agent, the time required for the etching to complete was longer when compared to HF [46]. Also, NH_4HF_2 intercalates NH_4^+ ions into the stacked layers thereby enabling the delamination of sheets without the need of delaminating agents. This phenomenon of intercalation of cations such as Na^+, K^+, $NH4^+$, Mg^{2+} and Al^{3+} into the MXene layers not only help in the delamination of the MXene sheets but also helps to increase the volumetric capacitance in case of supercapacitors. A schematic illustration of this is given in Fig. 4 [49].

Ghidiu et al. reported the use of fluoride salt, LiF dissolved in 6 M HCl as the etching solution. The Ti_3AlC_2 MAX powders were slowly added to the acid-salt mixture and the solution mixture was maintained at 40 °C for 45 h. The sediment was filtered and washed with DI water repeatedly. This sediment in its wet state was in a clay form and could be rolled to form flexible, free-standing films or the wet clay could be molded into different shapes. In its diluted state, it could also be used as an ink (shown in Fig. 5) [50].

It is known that the M—A bonds are comparatively easy to break when compared to M—X bonds, but it is imperative to note that the bond energies of different M—A elements varies widely. In particular, the bond energies associated with Ti-Al and Ta-Al in Ti_2AlC and Ta_2AlC MAX phases is 0.98 eV and 1.25 eV, respectively. This shows that strong etchants and longer etching times are required to etch Al from Ta_2AlC when compared to Ti_2AlC [44].

Nitride based MXenes are electronically conductive than carbide based MXenes, thus are suitable to be used as electrodes for supercapacitors. Aqueous acidic solutions are suitable for etching the A element from their MAX phase to produce carbide and carbonitride based MXenes, but fail to produce nitride based MXenes. Shein and Ivanovskii reported that the energy needed for the formation of $Ti_{n+1}N_n$ from its MAX phase $Ti_{n+1}AlN_n$ is higher when compared to $Ti_{n+1}C_n$ whereas the cohesive energy of $Ti_{n+1}N_n$ is less than $Ti_{n+1}C_n$ [51]. Higher formation energy implies that the Al atoms are more strongly bonded in nitride based MAX phases thus requiring more energy for its removal. Lower cohesive energy implies that nitride based MAX phases is less stable with a possibility that it might dissolve in HF solutions. Due to these before said reasons, the synthesis of nitride based MXenes is found to be difficult. Only few works have been reported on the successful synthesis of nitride based MXenes till date [52,53]. For the first time, Urbankowski et al. reported the synthesis of Ti_4N_3 using a eutectic molten salt mixture as the etchant. The eutectic fluoride salt mixture consisted of 59 wt% of KF, 29 wt% of LiF and 12 wt% of NaF. This salt mixture was added to the MAX phase Ti_4AlN_3 and heated at 550 °C for 30 min under Ar. The multilayered $Ti_4N_3T_x$ particles were further delaminated to produce few and monolay-

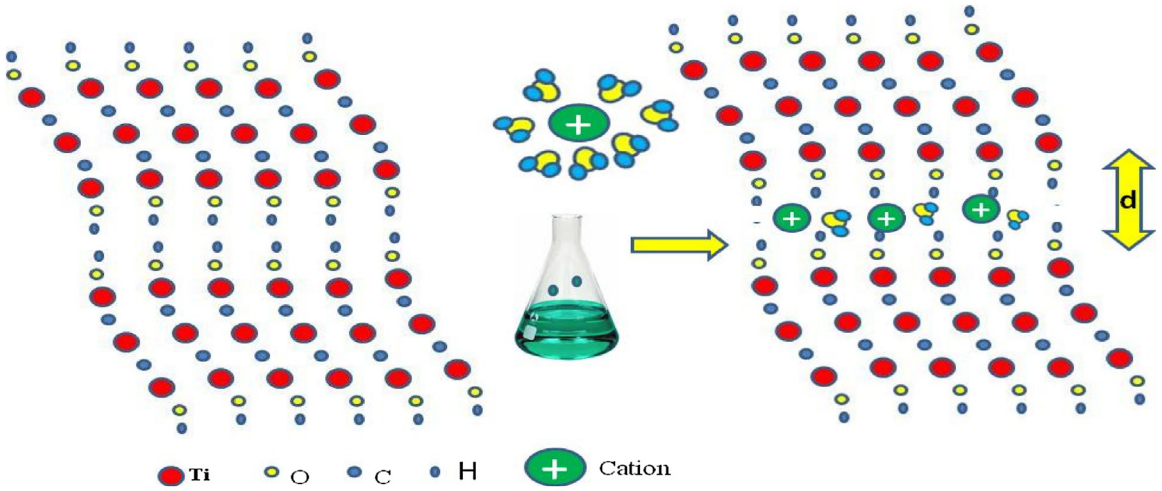

Fig. 4. Schematic illustration of the increase in the d spacing with intercalation of cations between $Ti_3C_2T_x$ layers.

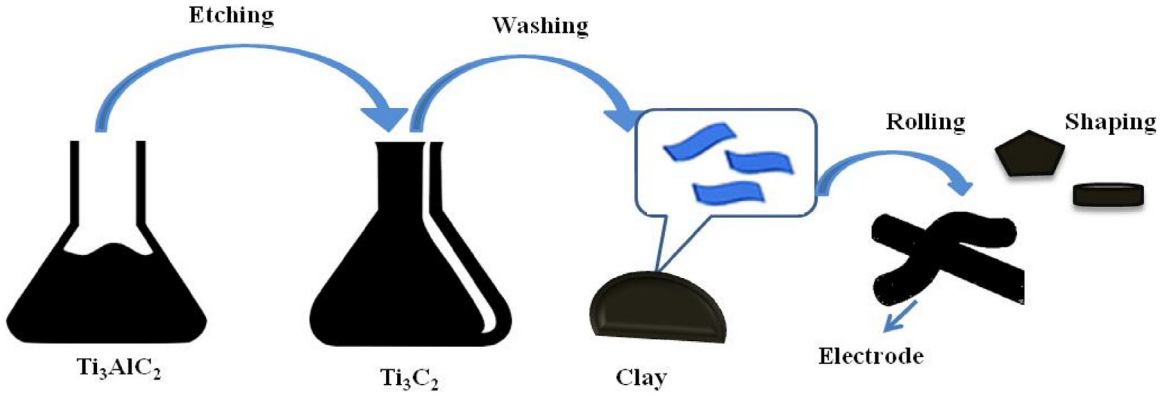

Fig. 5. Schematic of Ti_3C_2 MXene clay formed by etching Al from Ti_3AlC_2 using LiF-HCl as etching agents and electrode preparation using the wet clay. Clay is rolled up to obtain different shapes [50].

ered $Ti_4N_3T_x$ [52]. The XRD and the SEM images of the first nitride based MXene $Ti_4N_3T_x$ is given in Fig. 6. Soundiraraju and George reported the synthesis of lower order nitride based MXene Ti_2N as a Surface-Enhanced Raman Scattering substrate. Different etchants, viz., HF, HF–HCl, KF, and KF–HCl mixture were used in this study in order to determine the best suitable etchant. Typical layered morphology was observed through SEM images for Ti_2N obtained by immersing the MAX powders of Ti_2AlN into a mixture of KF and HCl [53]. Molten salt etching method has been found to be effective in forming nitride based MXenes. Very recently Djire and group have reported the formations of Ti_2N and Ti_4N_3 MXenes using the molten salt etching method [54,55].

2.2. Intercalating and delaminating agents

Intercalation and delamination/exfoliation is important to obtain single-layered MXene sheets. During the process of etching and delaminating, parameters such as surface functionalization, number of layers, crystallinity are all affected. As mentioned earlier, when fluoride salts such as KF, NaF or LiF dissolved in HCl is used as an etchant, additional delaminating agent is not required as the cations in the fluoride salts intercalate into the layers of MXene thereby delaminating them. Thus simultaneous exfoliation is achieved during the etching process. Delamination can simply be achieved by sonicating the MXene suspension, but prolonged sonication will have an effect on the edges of the lamellar structures and might break the sheets [49]. Mashtalir et al. for the first time reported on the intercalation of hydrazine monohydrate (HM) and hydrazine monohydrate dissolved in DMF into the layers of functionalized Ti_3C_2 and then delaminating them using urea and DMSO. It was seen that intercalation of HM and HM/DMF resulted in an increase in the c-lattice parameter of f-Ti_3C_2, from 19.5–25.48 and 26.8 Å, respectively. With the use of DMSO, the c-LPs increased from 19.5 ± 0.1 Å to 35.04 ± 0.02 Å. An increase in the c-lattice parameter indicates the increase in the interlayer spacing in multi-layered MXenes, which in turn leads to the weakening of bonds between the layers thereby enabling exfoliation of multi-layered MXenes into single- layered MXenes [56]. Fig. 7 indicates the FESEM images of MAX, etched MAX forming MXene and the delaminated structures. The c-lattice parameter increased with the etching of Al to 17.33 Å from 13.59 Å [53].

The zeta potential measurements show that MXenes are negatively charged (hydrophilic in nature) and thus when they are delaminated, they can form stable, surfactant free colloidal solutions in water. This phenomenon was well explained by Naguib et al., where various organic bases were tested for their effectiveness as delaminating agents [57]. Common delaminating agents are dimethyl sulfoxide (DMSO), tetramethylammonium hydroxide (TMAOH), urea, hydrazine, choline hydroxide and *n*-butylamine. Once the organic molecules intercalate into the MXene flakes, slight agitation or mild sonication will lead to the delamination of sheets (scheme shown in Fig. 8) [57,73,74]. High-energy mechanical milling method (HEMM) in organic solvents was proposed by Wu et al. wherein, the MXene powders were suspended in dimethyl

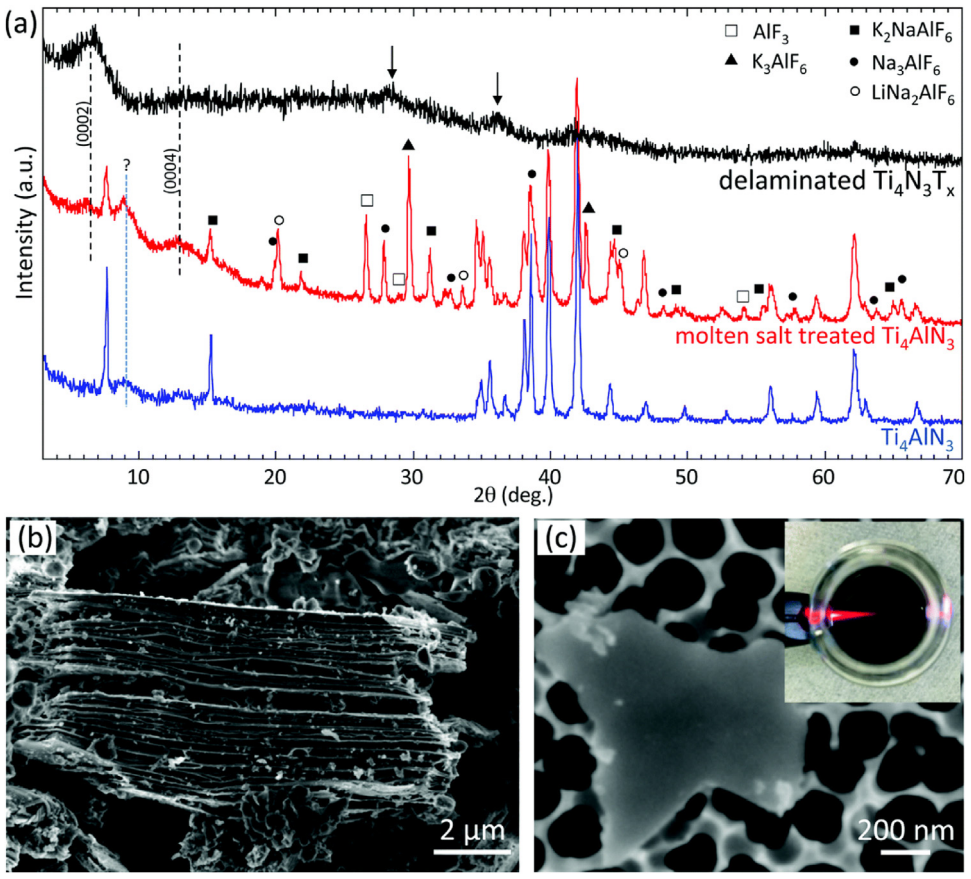

Fig. 6. (a) XRD patterns of Ti_4AlN_3, molten salt treated Ti_4AlN_3, and delaminated $Ti_4N_3T_x$. (b) SEM image of molten salt treated Ti_4AlN_3 at 550 °C for 0.5 h under Ar flow. (c) SEM image of few-layered $Ti_4N_3T_x$ particle on an alumina filter substrate. Reproduced with permission from [52] copyright 2016, The Royal society of Chemistry.

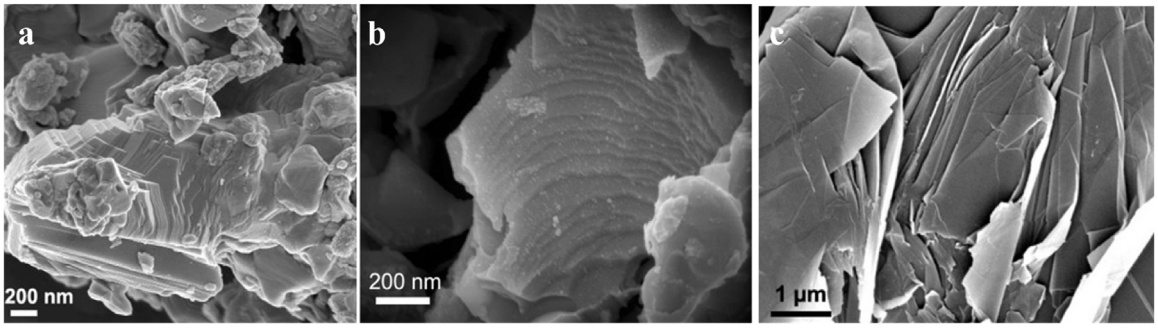

Fig. 7. FESEM images of Ti_2AlN MAX phase (a), KF-HCl etched MXene Ti_2N (b), delaminated MXene (c). Reproduced with permission from [53] copyright 2017, American Chemical Society.

sulfoxide (DMSO) and milled to produce few-layer nanosheets. These few-layer MXene nanosheets efficiently prevents the oxidation of MXene and facilitates fast electron transport, Na^+ diffusion and exhibits great performance as anodes for sodium-ion batteries [75] Table 1 provides a summary of trends used in the synthesis and exfoliation of MXenes.

2.3. Surface chemistry of MXene

MXenes have already established their importance in a myriad of applications such as sensors, catalysts, electromagnetic shielding, energy storage and many more. This achievement is greatly due to their high metallic conductivity. Thus research is being focused in further enhancing their metallic conductivity. This could be possible by engineering the surface chemistry of MXenes [76]. In the chemical formula of MXene $M_{n+1}X_nT_x$, T_x stands for surface terminations and x indicates the amount of terminations onto the surface. Thus surfaces contain species that does not belong to the MAX phase. The strong bond existing between the M atoms and the T_x groups is responsible for the negative energy formation of MXenes [77]. Persson demonstrated theoretically the termination process happening in MXenes. When HF interacts with the MAX phase Ti_3AlC_2, it targets the A layer in the MAX phase. HF dissociates into H and F and starts interacting with A and M elements. H being moderately attracted, escapes as H_2. Al reacts with F forming AlF_3, which is later removed by continuous washing. In this process M element gets terminated with H and F [78]. XPS is a powerful tool in determining the surface chemical compositions and the chemical states of the various species. This is the most popular technique reported in literature [56]. Another popular technique

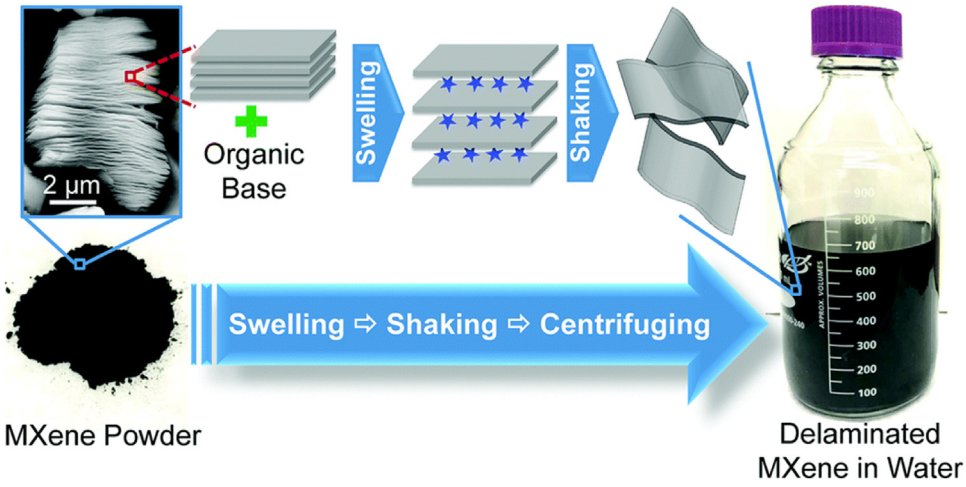

Fig. 8. Schematic for MXene delamination process by reacting MXenes with an organic base that causes multilayered MXene powder (pictured in bottom left) to swell significantly. Then by simply hand shaking or mild sonication in water the layers delaminate forming a stable colloidal solution (right side). A typical SEM image of the as synthesized Ti_3CNT_x multi-layer MXene is shown top left. Reproduced with permission from [57] copyright 2015, The Royal society of Chemistry.

Table 1
Summary of synthesis of MXene from MAX phases, exfoliating agents and their applications.

MAX phase	Etchant used for the synthesis	Etching Conditions (Concentration and time)	MXene	Delaminating agent used	Applications	Ref.
V_2AlC	HF	48 %, 92 h	V_2CT_x	TBAOH, n-butylamine, choline hydroxide	–	[57]
Ti_3AlCN	HF	30 % for 18 h	Ti_3CNT_x	TBAOH	–	[57]
Ti_3AlC_2	LiF/HCl	5M LiF and 6 M HCl	$Ti_3C_2T_x$	Ultrasonication	Anti-bacterial	[58]
Ti_3AlC_2	HF	40 %, 48 h	$Ti_3C_2T_x$	–	Electromagnetic absorption and shielding	[22]
Ti_3AlC_2	HF	48 %, 20 h	$Ti_3C_2T_x$	DMSO	Sensor	[59]
Ti_2AlC	HF	10 %, 18 h	Ti_2C	–	–	[60]
Mo_2Ga_2C	HF	48 – 51%, 6.6 days	Mo_2C	–	–	[60]
Ti_3AlC_2	LiF-HCl	9 g of LiF, 9 M HCl, 24 h	Ti_3C_2	DMSO	Supercapacitor	[61]
V_2AlC	NaF-HCl	2 g of NaF, 40 ml HCl	V_2C	–	Li – ion battery	[62]
Ti_3AlC_2	HF	50 %, 2 h	Ti_3C_2	–	–	[15]
Ti_3AlC_2	LiF-HCl	1 g of LiF, 20 ml HCl, 20 days	Ti_3C_2	–	Supercapacitor	[37]
Ti_2AlN	KF-HCl	6 g of KF, 6 M HCl, 1 h	Ti_2N	DMSO	SERS	[53]
Ti_4AlN_3	KF + LiF + NaF and H_2SO_4	Molar ratio 0.59 : 0.29 : 0.12	$Ti_4N_3T_x$	TBAOH	–	[52]
Ti_2AlN	KF + LiF + NaF and HCl	Molar ratio 0.59 : 0.29 : 0.12	Ti_2NT_x	–	Energy storage	[54]
$Hf_3(Al(Si))_4C_6$	HF	35 %, 60 h	$Hf_3C_2T_z$	–	Li – ion storage	[63]
Nb_2AlC	HF	50 %, 48 h	Nb_2C	Isopropylamine	Li – ion storage	[64]
Mo_2TiAlC_2	HF	48–51 %, 48 h	Mo_2TiC_2	DMSO	Li – ion storage	[65]
$Mo_2Ti_2AlC_3$	HF	48–51 %, 90 h	$Mo_2Ti_2C_3$	–	Li – ion storage	[65]
Ti_3AlC_2	NH_4F (hydrothermal)	150 ^{O}C, 24 h	Ti_3C_2	–	Li – ion storage	[66]
Ti_3AlC_2, Ti_2AlC	HCl + fluoride salt	20 ml HCl	Ti_3C_2, Ti_2C	DMSO, Urea, NH_3 H_2O	Methane absorption	[48]
Ti_3AlC_2	HF	50 %, 18 h	$Ti_3C_2T_x$	Hydrazine monohydrate	Supercapacitor	[67]
Ti_3AlC_2	HF	50 %, 2 h	$Ti_3C_2T_x$	Sonication	–	[68]
Ti_3AlC_2	HF	40 %, 18 h	$Ti_3C_2T_x$	DMSO	Supercapacitor	[69]
Ti_3AlC_2	HF	50 %, 36 h	$Ti_3C_2T_x$	DMSO	Supercapacitor	[70]
Ti_3AlC_2	HCl +HF + DI water	9 M, 49 %	$Ti_3C_2T_x$	LiCl	Supercapacitor	[71]
V_4AlC_3	HF	40 %, 24 and 96 h	V_4C_3	–	Supercapacitor	[72]
Ti_3AlC_2	HF	50 %, 96 h	$Ti_3C_2T_x$	–	Supercapacitor	[33]

- Indicate that the corresponding datas are not available.

is nuclear magnetic resonance (NMR). NMR is also used in the quantification of species. Other basic techniques include scanning electron microscope (SEM), transmission electron Microscope (TEM), energy-dispersive x-ray spectroscopy (EDX) and electron energy loss spectroscopy (EELS) [53]. However, EDX cannot detect lighter elements and depends largely on the experimental conditions. Hope et al. demonstrated that NMR technique is suitable for the quantification of surface terminations on the $Ti_3C_2T_x$ MXene [79]. When exposed to aqueous HF solutions, MXene surface gets saturated with oxygen at low hydrogen chemical potential μ_H. MXenes with M = Sc exhibits high stability with F terminations and is easy to be exfoliated to single layers [77]. Naguib et al. theoretically proved that surface termination and their orientation with respect to MXene sheets helps in tuning their band gap. They reported that Ti_3C_2 is metallic in nature but with terminations such as hydroxyl and/or fluorine groups induces a small band gap of 0.05 eV and 0.1 eV respectively [15,76]. Liu et al. reported that the surface chemistry of MXenes strongly affect their Fermi levels. When compared to bare MXenes, surfaces terminated with –O have increased work function, -OH terminations exhibit decreased work function and –F terminations exhibit values based on the material type. The surface dipoles along with Fermi level pinning allows

injection of Schottky-barrier-free charges into the 2D semiconductors [80].

3. Properties

Due to the various outstanding properties exhibited by MXenes, they find applications in various fields. The electronic properties of MXenes are influenced by their composition and the functional groups attached onto their surfaces. Transition metal carbides and Transition metal nitrides are known to possess superior chemical and thermal stability [81]. This also implies to MXenes due to the strong M—C and/or M—N bonds present in them. The first report on experimental determination of the thermal stability of Ti_3C_2 MXene was given by Li *et al* [38]. In their study, thermogravimetry and differential scanning calorimetry analysis was carried out based on which the stability was determined. In the presence of Argon, Ti_3C_2 MXene was stable upto a temperature of 800°C whereas in the presence of oxygen, parts of MXene were oxidized at 200°C forming nano crystals evenly distributed on the surface of the sheets and at 1000°C, MXene sheets were completely oxidized. This shows that MXenes are unstable in oxygen environment and in water [82]. Delaminated MXenes in water form colloidal solutions and these can be stored in hermetic Ar-filled bottles to avoid oxidation. Degradation usually starts at the edges forming crystals and then spreads exponentially [83].

A flexible free standing conductive film was prepared for the first time using Ti_3C_2T composite with poly(diallyldimethylammonium chloride) (PDDA) and polyvinyl alcohol (PVA) by Ling et al. A $\tilde{3}$.3-μm-thick $Ti_3C_2T_x$ film exhibited a tensile strength of 22 ± 2 MPa and a Young's modulus of 3.5 ± 0.01 GPa. With a 60 % PVA added to the MXene, the tensile strength increased to about four times when compared to pure $Ti_3C_2T_x$ film. For pure $Ti_3C_2T_x$, an electrical conductivity of about 2.4×10^5 S/m was observed, whereas $Ti_3C_2T_x$/PVA composite film exhibited an electrical conductivity of 2.2×10^4 S/m. Addition of polymer matrix into the structures of MXenes have shown to exhibit enhanced mechanical and electrical properties [84]. Transparent conductive thin films were produced by spray coating of colloidal suspensions of delaminated $Ti_3C_2T_x$ whose optoelectronic properties were studied. It was seen that these properties vary with the intercalations of ions between the layers of $Ti_3C_2T_x$. Thin films from MXene can also be made by spin coating or drop casting methods [85,86]. Magnetism is said to be present in MXenes which do not have surface terminations, however such MXenes do not predominantly exist. Khazaei et al. proposed that Cr based MXenes such as Cr_2CF_2, $Cr_2C(OH)_2$, Cr_2NF_2, $Cr_2N(OH)_2$, and Cr_2NO_2 with surface terminations can be magnetic at low temperatures, however there is no experimental evidence till date for their magnetic properties [87].

Though more than 60 MAX phases are reported, only few MXenes have been found from them and have found their practical applications. Many more MXenes are expected to be practically used in the near future. Carbide and carbonitride based MXenes such as Ti_2C [41], Ti_3C_2 [50], V_2C [62], Nb_4C_3 [88], Nb_2C [89], Mo_2ScC_2 [90], Mo_2C [91], Zr_3C_2 [92], Ta_4C_3 [41], $Hf_3C_2T_z$ [48], TiNbC [73], Mo_2TiC_2 [65], $(Ti_{0.5}Nb_{0.5})_2C$ [41], $(V_{0.5}Cr_{0.5})_3C_2$ [73], Cr_2TiC_2 [65], $Mo_2Ti_2C_3$ [65], $(Nb_{0.8}Ti_{0.2})_4C_3$ [88], $(Nb_{0.8}Zr_{0.2})_4C_3$ [88] and Ti_3CN [57] are some of the reported MXenes. Nitride-based MXenes viz. Ti_4N_3 [52] and Ti_2N [53] have also been reported. Metal nitride based MXenes obtained by the ammonization of carbide based MXenes have also been reported [93]. The unique electrical and mechanical properties, thermal and chemical stability led to the use of these MXenes in various fields such as electrochemical energy storage systems such as batteries and supercapacitors, sensors, catalysis, electronics, electromagnetic interference shielding, fuel cells and so on.

4. Applications

4.1. Batteries

Most of the MXenes reported till date has found their importance as electrode materials in Li-ion batteries (LIBs). The work reported by Naguib et al. opened doors for the use of MXene (Ti_2C) in LIBs [34]. Ti_3C_2 intercalated with DMSO pose higher capacity than that before intercalation. Intercalated Ti_3C_2 exhibited a capacity of 123.6 $mAhg^{-1}$ at a rate of 1 C and an efficiency of about 47 %. These values are higher than that of 2D Ti_2C [94]. Kim et al. investigated the effect of high mass loading onto the electrodes for LIBs. When $Ti_3C_2T_x$ discs with a density of 2.52 gcm^{-3} was used as an anode for LIBs, an initial reversible areal capacity of 15 $mAhcm^{-2}$ was obtained, which later decreased to 5.9 $mAhcm^{-2}$ after 50 cycles but with the use of Nb_2C as the electrode material, the initial capacity of 16 $mAhcm^{-2}$ decreased to 6.7 $mAhcm^{-2}$ after 50 cycles. This shows that the capacity observed in Nb_2C is much better than that seen in $Ti_3C_2T_x$ and this is due to the ease intercalation of Li ions into the thinner layers of M_2C when compared to M_3C_2 MXenes [95]. MXene composites such as MoS_2/MXene, Ti_3C_2/Reduced Graphene Oxide, Fe_3O_4/Ti_3C_2 have also been widely researched as electrodes for Li-ion batteries [96–98]. Zhu et al. investigated the structural and energy storage properties of Li decorated Zr_2C and Zr_2CS_2 through DFT analysis. The diffusion barrier is reduced in Zr_2CS_2 when compared to Zr_2CO_2 while maintaining the same specific capacity [99]. MXenes such as Zr_2C, Zr_3C_2, Zr_2CO_2, $Zr_3C_2O_2$, Ti_3C_2 MXene/CNTcomposites were all proven to be suitable for Na ion batteries [36,100,101].

4.2. Supercapacitors

With well defined geometry, large surface areas and layered structures, MXenes have found to be potential candidates for a myriad of applications. MXenes posses outstanding properties such as extreme hardness, resistance to oxidation, hydrophilicity, capability to accommodate various intercalants, high melting point and thermal conductivity [49,102]. The tiny amounts of energy obtained from renewable sources such as solar and wind needs to be converted into electrochemical energy and stored effectively. Supercapacitor, the new generation electrochemical storage device is devoted in effectively storing the tiny amounts of energy. In the process of exploring new electrode materials for the construction of supercapacitors, MXenes and their composites which pose the above said properties are found to be suitable in storing energy efficiently [140].

Lukatskaya et al. reported the effect of electrochemical intercalation of cations such as Na^+, K^+, NH_4^+, Mg^{2+}, and Al^{3+} on the storage capabilities of Ti_3C_2 MXene. Ti_3C_2 MXene was placed in various aqueous salt solutions to achieve spontaneous intercalation of cations. With such intercalations, Ti_3C_2 electrode exhibited an increase in capacitance of about 300 Fcm^{-3}. The obtained capacitance values were greater than that of porous carbon materials. These results enabled researchers on focusing the use of MXenes in supercapacitors [49]. Ti_3C_2 is the widely researched MXene till date and it is shown to exhibit pseudocapacitive nature [103]. Hu et al. reported the fundamental mechanism happening in $Ti_3C_2T_x$ with acidic electrolytes. With the help of in situ Raman spectroscopy, the charge/discharge processes happening in $Ti_3C_2T_x$ electrodes in different sulfate ion containing electrolytes (H_2SO_4, $(NH_4)_2SO_4$ and $MgSO_4$) were studied. It was observed that the hydronium in H_2SO_4 bonds or debonds with the oxygen atoms present on the surface of $Ti_3C_2T_x$ upon charging or discharging the pseudocapacitor in acidic electrolyte. Whereas in $(NH_4)_2SO_4$ and $MgSO_4$ EDLC was observed [104].

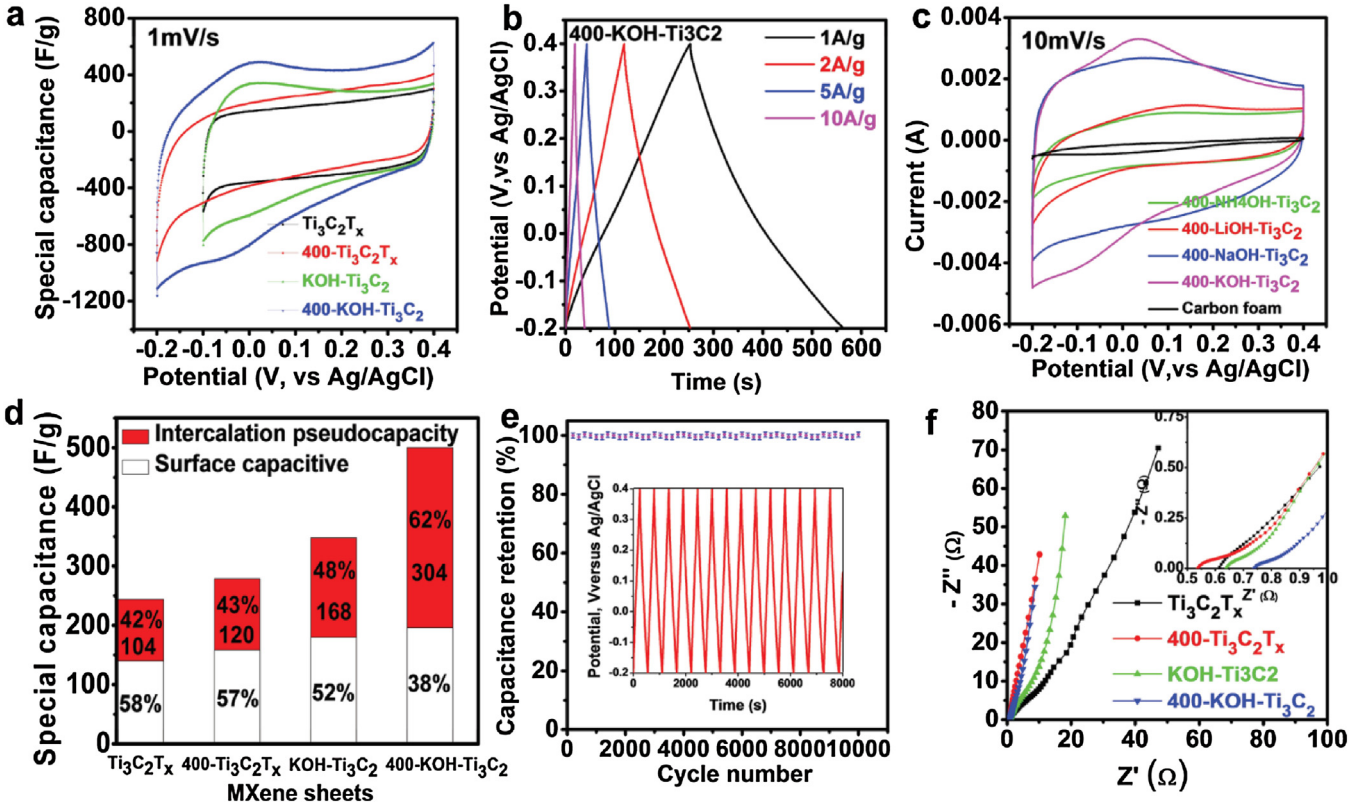

Fig. 9. Electrochemical performance of MXene and surface modified MXene electrodes in three-electrode system. a) Cycle voltammetry profiles at 1 mVs^{-1} for different MXene-based electrodes in 1 m H_2SO_4. b) The galvanostatic charge/discharge curves for 400-KOH-Ti_3C_2 MXene sheets at current densities of 1, 2, 5, and 10 Ag^{-1}. c) Cyclic voltammetry profiles at 10 mV s^{-1} for other cation intercalation MXene sheets with lowest terminal groups. d) Comparison of capacitance for MXene sheets (at scan rate of 1 mV s^{-1}). The total capacitance is separated into intercalation pseudocapacity and surface capacitive contributions (the inset numbers 104, 120, 168, and 304 point to the part of intercalation pseudocapacity). e) Capacitance retention test of 400-KOH-Ti_3C_2 electrode in 1 m H_2SO_4 (the blue lines were error bars). Inset shows galvanostatic cycling data collected 1 Ag^{-1}. f) Electrochemical impedance spectroscopy data of different MXene-based electrodes. The inset in (f) shows the magnified high-frequency region. Reproduced with permission from [106] copyright 2017, WILEY-VCH.

$Ti_3C_2T_x$ loaded on silk derived carbon cloth was used as an electrode material for the fabrication of flexible supercapacitors. It exhibited an areal capacitance of 362 $mFcm^{-2}$ with excellent flexibility and cyclic stability [37]. MXene based supercapacitors have all shown to poses excellent cyclic stability due to their strong M—X bond and superior specific capacitance [69,70,84,105–109]. Dall'Agnese et al. reported the effect of chemically modified surfaces of $Ti_3C_2T_x$ MXenes with DMSO. The oxygen terminations onto the surfaces aided in improving the specific capacitance of these materials. When tested in H_2SO_4 acid electrolyte, $Ti_3C_2T_x$ MXene exhibited a capacitance of 415 Fcm^{-3} at 5 Ag^{-1} with no significant degradation happening upto 10,000 cycles. [110] Ghidiu et al. reported the clay like $Ti_3C_2T_x$ which could be molded into any possible shape. Clay like paste was obtained which was rolled in its wet form to obtain flexible films (Fig. 5). This eases the techniques of intercalation, delamination and filtration. The film when tested for its supercapacitor performance in H_2SO_4 exhibited a specific capacitance of 245 Fg^{-1} with no capacitance loss even after 10,000 cycles. The improved performance exhibited by the clay like $Ti_3C_2T_x$ rolled films was attributed to the smaller size of H^+ compared to other cations and the accessibility to the interlayer space due to the pre-intercalated water [50].

Li et al. reported an improved gravimetric capacitance of $Ti_3C_2T_x$ MXene compared to its previous reported value (245 Fg^{-1}). By modifying the surface of MXene and by intercalating cations such as K^+, a higher density of 27.4 $WhKg^{-1}$ can be obtained making them the most suitable candidate for supercapacitor electrodes. Ti_3AlC_2 powders were suspended in solutions of HF to remove Al forming Ti_3C_2. As a result of etching, -OH and -F groups were terminated onto the MXene surfaces. Ti—F bond is unstable in basic solutions; thus KOH was chosen to replace the -F terminated functional groups with –OH groups. Basic salt treated MXene was calcined at higher temperatures to modify the surface terminations and intercalate K^+ cations. The c-lattice parameter increases in such a case thereby increasing the inter-layer distances. A gravimetric capacitance of 517 Fg^{-1} at a discharge rate of 1 Ag^{-1} was obtained with a capacitance retension of about 99 % after 10,000 cycles. The electrochemical performance of surface modified and cation intercalated Ti_3C_2 MXene is depicted in Fig. 9 [106].

4.2.1. *MXene composites for supercapacitors*

To further enhance the properties exhibited by MXenes and to improve their capacitive properties, MXenes were made composites with various other materials. Materials such as metal oxides, carbonaceous and polymers were made composites with MXenes. Xu et al. reported the synthesis of MXene/graphene fibers using the synergistic effect existing between liquid crystals of graphene oxides and MXene sheets. The Ti_3C_2 MXene/GO mixture was injected through a nozzle into a coagulation bath containing DI water and 5 wt% $CaCl_2$. Due to the coulombic force interlinking the negative MXene sheets and GO layers, MXene/GO fibers were obtained. These fibers were assembled into a two electrode device and tested for its electrochemical properties. With 1 M sulfuric acid as an electrolyte, a specific capacitance of 890.7 Fcm^{-3} at 10 mV/s was obtained. Flexible supercapacitor was constructed with a PVA/H_3PO_4 gel solid state electrolyte and it exhibited a specific capacitance of 586.4 Fcm^{-3} at 10 mV/s. In addition to the electric double layer surface adsorption happening due to the GO layers,

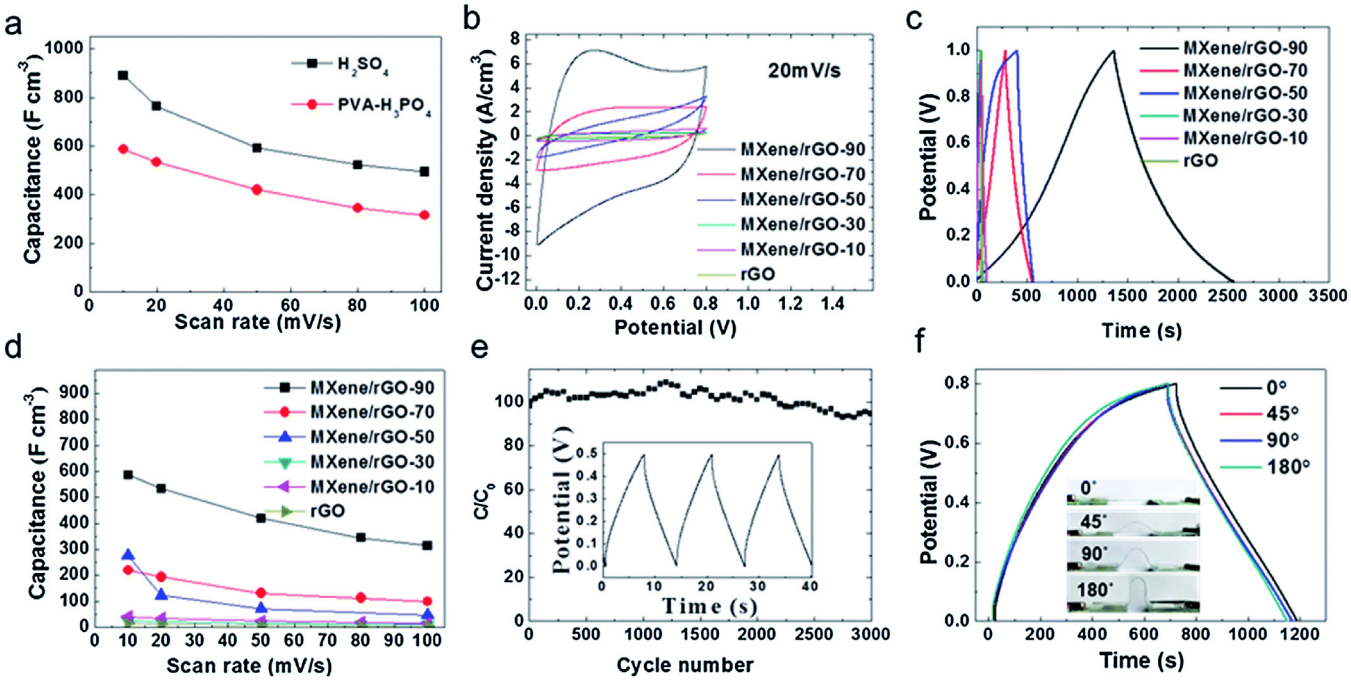

Fig. 10. Comparison of volumetric capacitances of MXene/rGO-90 fiber based FSCs in 1 M liquid H_2SO_4 and solid PVA–H_3PO_4 electrolytes at different scan rates (a); CV curves (at 20 mV s^{-1}) (b), GCP curves (at 0.2 mA cm^{-2}) (c), volumetric capacitances at different scan rates (d) of the fabricated solid state MXene/rGO FSCs with various MXene contents (0, 10, 50, 70, and 90 w/w%); cycling stability (at 2 mA cm^{-2}) of the solid state MXene/rGO-90 fiber based FSCs (e); bending property of solid state MXene/rGO-77 based FSCs at different bending angles (f). Reproduced with permission from [61] copyright 2017, The Royal Society of Chemistry.

Ti atoms involve in redox reactions accounting for pseudocapacitance. Hence these composites exhibit improved electrochemical behavior as shown in Fig. 10 [61].

MXene Ti_3C_2/carbon fiber composite prepared through electrospinning technique exhibited excellent supercapacitive behavior [71]. The few layered MXene flakes were dispersed in DMF mixed with polyacrylonitrile and then loaded into a syringe as shown in Fig. 11. Due to the difference in the voltage potentials applied between the tip of the needle and the copper plate onto which the fibers were collected, MXene/PAN composite fibers were derived. These fibers were carbonized at high temperatures to obtain MXene/carbon nanofibers. Fibers carbonized at 800 ^{O}C composite with MXene exhibited a specific capacitance of 239 $mFcm^{-2}$.

Wang et al. reported the use of liquid phase exfoliation method to grow a 3D layer of nickel-aluminum layered double hydroxide platelets (LDH) on the exfoliated MXene Ti_3C_2. The 3D LDH network aids in establishing a fast pathway for ion movement and providing a large surface area for redox reactions. The conductive MXene substrate helps in improving the electrical conductivity. MXene/LDH composite exhibits a specific capacitance of 1061 Fg^{-1} at a current density of 1 Ag^{-1} with capacitance retention of about 70 % after 4000 cycles. The electrochemical performance of the composite electrode is shown in Fig. 12 [69].

An all-pseudocapacitive asymmetric device was fabricated by combining titanium carbide MXene ($Ti_3C_2T_x$) as the negative electrode and RuO_2 as the positive electrode. The asymmetric device operated with a wide window of 1.5 V, which is about two times when compared to that of symmetric supercapacitors. The asymmetric devices exhibited an excellent energy density of 37 $\mu Whcm^{-2}$ at a power density of 40 $mWcm^{-2}$ with excellent capacitance retention. These results show that the traditional carbon based materials used as negative electrodes in asymmetric supercapacitors can be replaced with MXenes [111]. Zhu et al. demonstrated the use of polypyrrole (PPy)/ MXene composite as supercapacitor electrodes. It is known that conducting polymers suffer from poor mechanical stability and limited capacitance. The practical applications of freestanding PPy films are thus greatly affected. To overcome these disadvantages, PPy is made composites with Ti_3C_2 MXene by intercalating PPy into layered Ti_3C_2 (l-Ti_3C_2) as shown in Fig. 13. Layered Ti_3C_2 helps in preventing the stacking of PPy and the bonds between the PPy and l-Ti_3C_2 provide efficient pathways for ion transport thereby providing good conductivity. An increase in capacitance of about 30 % and capacitance retension of 100 % was obtained after 20,000 cycles. The fabricated supercapacitor shows a capacitance of 35 $mFcm^{-2}$ and good bending and cycling performance [112].

Wen et al. reported the increase in the c lattice parameter of $Ti_3C_2T_x$ MXene sheets from 1.92 nm to 2.46 nm with the introduction of Nitrogen heteroatom in the MXene structure. MXenes were treated in ammonia gas at varying temperatures of 200, 300, 500 and 700 °C for 2 h in a tube furnace. N atoms replace the C atoms in $Ti_3C_2T_x$ thereby increasing the interlayer distances in the MXenes. N-$Ti_3C_2T_x$ MXenes had an increase of about 46 % in its gravimetric capacitance compared to the undoped $Ti_3C_2T_x$. The composite electrodes exhibited a specific capacitance of 192 Fg^{-1} in 1 M H_2SO_4 and 82 Fg^{-1} in 1 M $MgSO_4$ electrolyte [113].

4.3. Catalyst

Noble metal such as platinum is widely used as catalyst in fuel cells and many other reactions. There is a strong need to find a low cost alternative to such a catalyst. MXenes are now being effectively used as photo and electrocatalysts. In the work reported by An et al., Ti_3C_2 and Pt were used as co-catalysts to enhance the photoactivity of g-C_3N_4 for H_2 production. Compared to the use of pure Ti_3C_2 or pure Pt as catalysts, the Ti_3C_2-Pt provided increased activity. This increased activity was attributed to the functional groups present onto the surface of the 2D sheets. The hydrogen evolution rate with the use of such a dual co-catalyst was about 5.1 mmol $h^{-1}g^{-1}$ [111]. MXenes such as Ti_2C, V_2C and Ti_3C_2 have oxygen and hydroxyl atoms onto their surface and such atoms act as catalytic active sites for the hydrogen evolution. This phe-

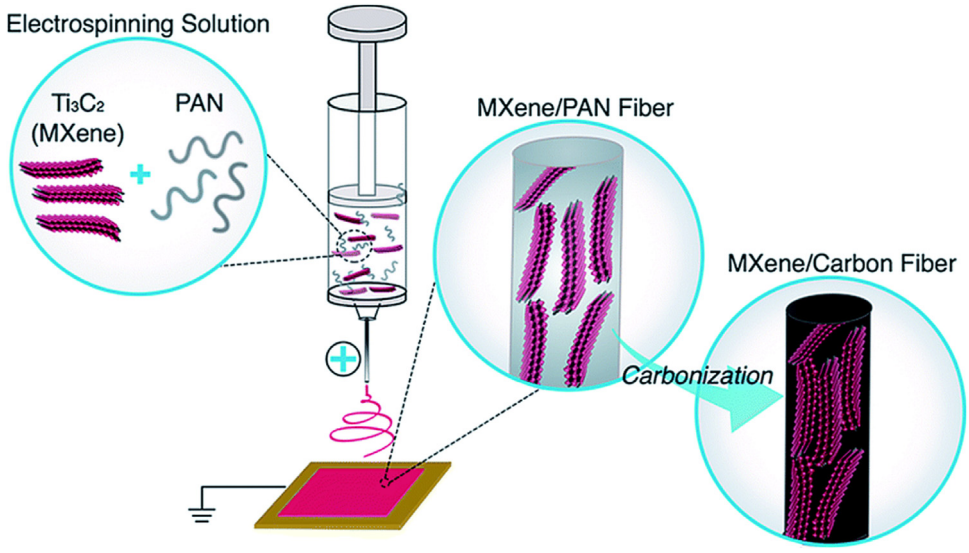

Fig. 11. Schematic of the production of $Ti_3C_2T_x$ MXene/carbon nanofibers via electrospinning. Reproduced with permission from [71] copyright 2019, The Royal Society of Chemistry.

nomenon was demonstrated by Gao et al. through DFT calculations [114]. Pan also predicted that, surface terminations are a critical parameter to enhance the catalytic activity of MXenes. The performance of hydrogen evolution depends on the composition, ability for hydrogen absorption and the functional groups attached onto the surface [115]. The hydrogen absorption energy will vary for different metals and the number of metal layers in the MXene, thus by tuning the layers in the MXenes, the HER activity can be controlled [116]. Reduction of CO_2 into hydrocarbons can help in reducing the green house effect. From the wide computational and experimental results available for Ti_2CT_2, it is known to possess extremely high carrier mobility and appropriate bandgap useful for photocatalysis. For the reduction of CO_2, Ti_2CO_2 was found to be the best catalyst through DFT computations and this was again attributed to the surface terminations onto the MXene [117]. Thus MXenes are mainly used as catalysts for reduction of CO_2, oxygen reduction reaction (ORR), oxygen evolution reaction (OER) and hydrogen evolution reaction (HER) [118].

4.4. Sensors

MXene acts as an adsorber for various gases and thus can be effectively used in gas sensing applications. This was confirmed through first principles simulations by Yu et al. wherein, different gases like NH_3, H_2, N_2, CH_4, CO, CO_2, NO_2 and O_2 were tested for their adsorbance onto the surface of Ti_2CO_2 monolayer. Among all the gases, NH_3 chemisorbed on Ti_2CO_2 with a charge transfer of 0.174 e. With the tuning of the applied strain on the MXene sheets, adsoption or release of NH_3 can be done [31]. High signal to noise ratio can be obtained in solid-state $Ti_3C_2T_x$ MXene gas sensors. Highly sensitive sensors with a detection limit of 50−100 ppb for volatile organic compounds was obtained. The hydroxyl group terminated Ti_3C_2 helps to strongly bind with analytes and the MXenes itself possess high metallic conductivity leading to low noise [119]. Nanoscale MXenes have also been explored for immobilization of Hb proteins and fabrication of mediator-free biosensors. These nano MXenes have enhanced surface area thereby providing more active sites for protein binding [30]. Rakhi et al. fabricated an amperometric glucose biosensor which exhibited stability, reproducibility and repeatability. These sensors were produced by immobilizing glucose oxidase (GOx) enzyme on Nafion solubilized Au/MXene nanocomposite over glassy carbon electrode (GCE) [120]. Ma et al. for the first time reported on fabrication of flexible and sensitive piezoresistive sensor by tuning the interlayer distances of MXene under an external pressure. These sensors were used to monitor subtle human activities [121].

4.5. Environmental remediation

The effluents obtained from various industries such as electroplating, metal finishing, leather tanning and pigment industries contain high amounts of toxic Cr (VI) ions. By the solvothermal alcoholysis of MXene (Ti_3C_2) in $FeCl_3$ solution, MXene derived urchin like 2D TiO_2–C/TiC nanomaterial was obtained. This nanomaterial has a high Cr(VI) ion adsorption ability of 225 mg/g [122]. Compared to multilayered $Ti_3C_2T_x$ MXenes, delaminated $Ti_3C_2T_x$ MXenes exhibits higher and faster Cu adsorption when exposed to water with copper metal ions as impurities. The delaminated $Ti_3C_2T_x$ MXenes have an adsorption capacity about 2.7 times greater than the commercially used activated carbon. The hydrophilic nature of MXene and the negatively charged surface functional groups greatly influences the adsorption of Cu ions [123]. A similar phenomenon was observed in the work reported by Peng et al., wherein adsorption of lead took place due to the presence of hydroxyl group on the surface of 2D titanium carbide [124]. 2D MXene-iron oxide composite prepared by intercalating magnetic ferric oxide into the layers of MXene was used in environmental remediation to separate phosphate ions in water [125]. Many reports on the use of MXene materials for environmental remediation, useful for mankind can be found in literature [82,126,127].

4.6. Other applications

The unique 2D structures have found applications in every possible field. Apart from the above said applications, MXenes have been found useful in shielding the electromagnetic interferences [22,128–130], lubricants [131], transparent conductive films [46,132,133], antibacterial activity [58,134,135], biomedical [74,136,137] and electronics [138,139]. In all these applications, MXenes have shown to outperform the existing conventional materials.

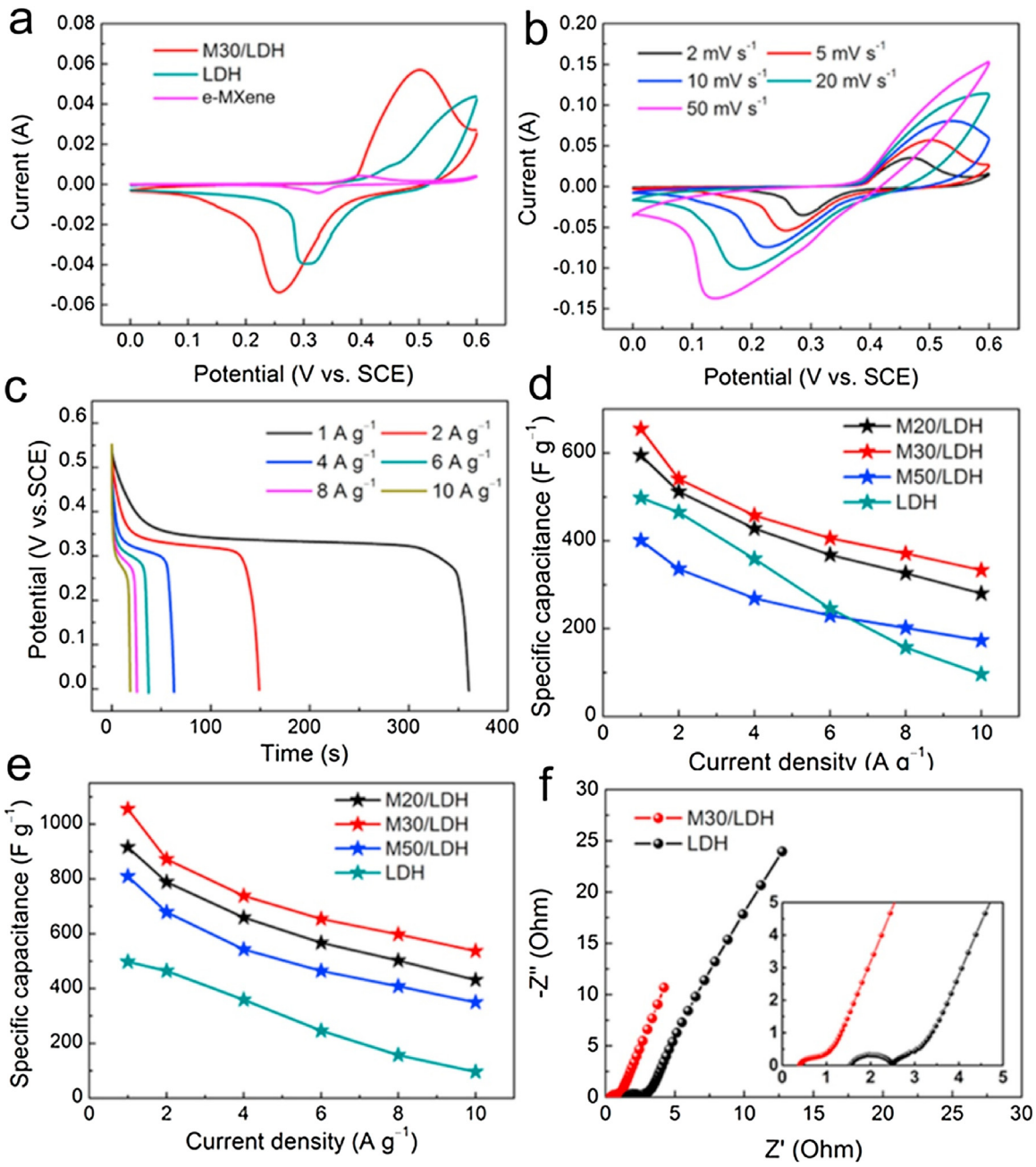

Fig. 12. (a) CV curves of e-MXene, LDH and the M30/LDH at a scan rate of 5 mVs^{-1} in 6 M KOH. (b) CV curves of M30/LDH at different scan rates. (c) The discharge curves of M30/LDH at different current densities based on the whole composite mass. Specific capacitance of LDH, M20/LDH, M30/LDH and M50/LDH at different current densities (d) based on the composite mass (e) based on LDH. (f) Nyquist plots of M30/LDH and LDH. Reproduced with permission from [69] copyright 2016, Elsevier Ltd.

5. Summary and outlook

To summarize, the recent trends in the synthesis of the 2D super material MXenes is well discussed. Among the various available MXenes, Ti_3C_2 is the most explored MXene. A myraid of etchants that are widely used for the etching of the A element from the MAX phases leading to the formation of MXenes is also discussed. The intercalation happening with the use of acid- salt mixtures as etchants leading to simultaneous delamination in the absence of a delaminating agent is well explained. Intercalation influences the interlayer distance thereby increasing the c-lattice parameter, which is important for energy storage devices. Aqueous solutions of HF fail to produce nitride based MXenes due to their stability constraints and their tendency to dissolve in HF. The composition and the functional groups attached onto the surface of MXene plays a major role in determining its electronic, optical, mechanical and magnetic properties. From DFT simulations, it was shown that MXenes with no terminations exhibited magnetic properties, but this is not experimentally proved yet. Thinner the layers of MXene, easy is the intercalation of Li- ions in a Li-ion battery leading to increased storage capacity. Thus mass loading onto the electrodes of a battery has a direct effect on its capacity. Also, dopants increase the capacity of the Li-ion battery. Various materials such as $Ti_3C_2T_x$, Ti_2CT_x, and V_2CT_x, have been investigated as electrode materials for supercapacitors. Of these materials, $Ti_3C_2T_x$ is the widely reported electrode material. The intercalation/ deintercalation of cations happening between the layers of MXene have a major contribution in energy storage applications. MXene can effectively be

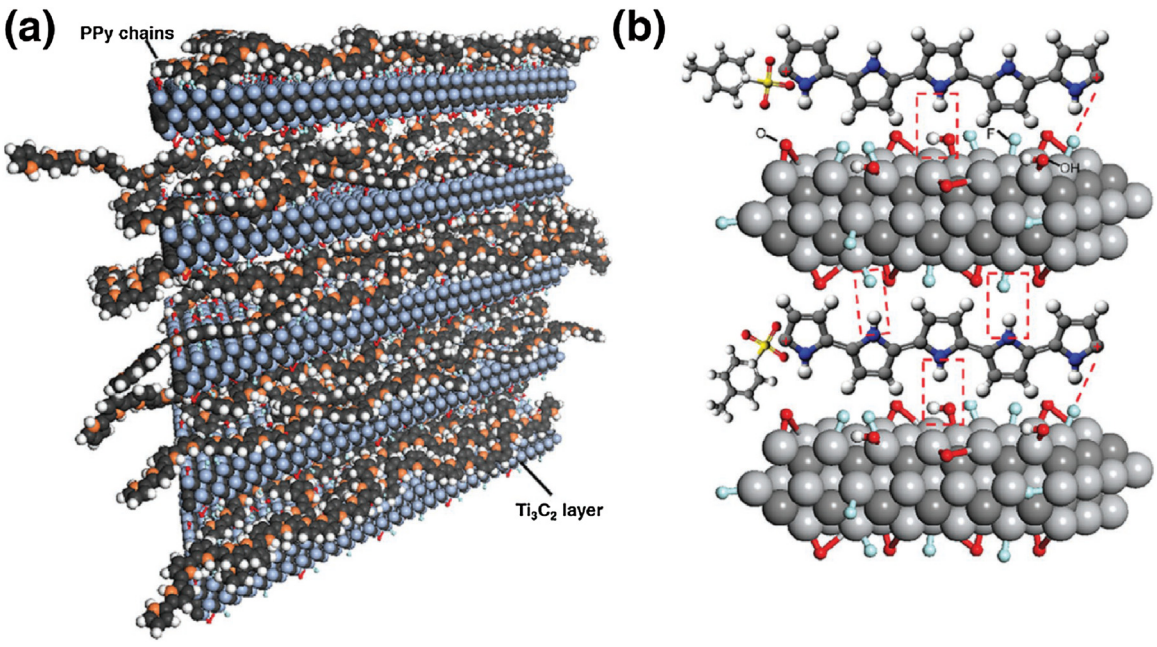

Fig. 13. a) Schematic of intercalated PPy in the interlayers of l-Ti_3C_2 and b) atomic-scale schematic of intercalated PPy in the interlayers of l-Ti_3C_2. Reproduced with permission from [112] copyright 2016, WILEY-VCH Verlag GmbH & Co.

used as the negative electrode in the asymmetric supercapacitors thereby replacing activated carbon. The surface terminated functional groups help in providing active sites for reactions and thus MXene pose as better catalysts. With the use of MXene electrodes in sensors, the S/N ratio is greatly improved and this is again attributed to the presence of surface terminations. MXenes have found its use in adsorbing various toxicities such as lead, chromium, copper that exists in water. Many more exciting developments with the use of MXenes are to be observed in future.

Many MAX phases have been theoretically proved to exist through computations, but experimental evidence for such MAX phases and the study of new MXenes from them is necessary. Till date only two reports have been found on nitride based MXenes, leaving it the less explored one. New routes for the experimental synthesis of nitride based MXenes with different metals is to be identified. Practical evidence pertaining to the electrical, thermoelectrical and magnetic properties of MXenes is needed.

Declaration of Competing Interest

The authors declare that they have no known competing financial interests or personal relationships that could have appeared to influence the work reported in this paper.

References

[1] Z. Salele Iro, A brief review on electrode materials for supercapacitor, Int. J. Electrochem. Sci. 11 (2016) 10628–10643.
[2] G. Wang, L. Zhang, J. Zhang, A review of electrode materials for electrochemical supercapacitors, Chem. Soc. Rev. 41 (2012) 797–828.
[3] S.-J. Park, M.K. Seo, Chapter 5 - interface applications in nanomaterials, in: S.J. Park, M.-K. Seo (Eds.), Interface Science and Technology, Elsevier, 2011, pp. 333–429.
[4] Q. Ke, J. Wang, Graphene-based materials for supercapacitor electrodes – a review, J. Mater. 2 (2016) 37–54.
[5] M.M.M. Ahmed, T. Imae, Chapter 10 - graphene-based nanolayers toward energy storage device, in: T. Imae (Ed.), Nanolayer Research, Elsevier, Amsterdam, 2017, pp. 353–389.
[6] G.A. Snook, P. Kao, A.S. Best, Conducting-polymer-based supercapacitor devices and electrodes, J. Power Sources 196 (2011) 1–12.
[7] K.S. Novoselov, A.K. Geim, S.V. Morozov, D. Jiang, Y. Zhang, S.V. Dubonos, I.V. Grigorieva, A.A. Firsov, Electric field effect in atomically thin carbon films, Science. 306 (2004) 666–669.
[8] W. Choi, I. Lahiri, R. Seelaboyina, Y.S. Kang, Synthesis of graphene and its applications: a review, Crit. Rev. Solid State Mater. Sci. 35 (2010) 52–71.
[9] M.J. Allen, V.C. Tung, R.B. Kaner, Honeycomb carbon: a review of graphene, Chem. Rev. 110 (2010) 132–145.
[10] K.S. Novoselov, D. Jiang, F. Schedin, T.J. Booth, V.V. Khotkevich, S.V. Morozov, A.K. Geim, Two-dimensional atomic crystals, Proc. Natl. Acad. Sci. U. S. A. 102 (2005) 10451–10453.
[11] M. Chhowalla, Z. Liu, H. Zhang, Two-dimensional transition metal dichalcogenide (TMD) nanosheets, Chem. Soc. Rev. 44 (2015) 2584–2586.
[12] L. Ma, C. Abney, W. Lin, Enantioselective catalysis with homochiral metal–organic frameworks, Chem. Soc. Rev. 38 (2009) 1248–1256.
[13] S. Jiang, M.Q. Arguilla, N.D. Cultrara, J.E. Goldberger, Covalently-controlled properties by design in group IV graphane analogues, Acc. Chem. Res. 48 (2015) 144–151.
[14] H. Liu, A.T. Neal, Z. Zhu, Z. Luo, X. Xu, D. Tománek, P.D. Ye, Phosphorene: An Unexplored 2D Semiconductor with a High Hole Mobility, ACS Nano 8 (2014) 4033–4041.
[15] M. Naguib, M. Kurtoglu, V. Presser, J. Lu, J. Niu, M. Heon, L. Hultman, Y. Gogotsi, M.W. Barsoum, Two-dimensional nanocrystals produced by exfoliation of Ti_3AlC_2, Adv. Mater. 23 (2011) 4248–4253.
[16] M. Dahlqvist, B. Alling, J. Rosén, Stability trends of MAX phases from first principles, Phys. Rev. B 81 (2010), 220102.
[17] M.W. Barsoum, The $M_{N+1}AX_N$ phases: a new class of solids: thermodynamically stable nanolaminates, Prog. Solid State Chem. 28 (2000) 201–281.
[18] M. Naguib, V.N. Mochalin, M.W. Barsoum, Y. Gogotsi, 25th anniversary article: MXenes: a new family of two-dimensional materials, Adv. Mater. 26 (2014) 992–1005.
[19] M.W. Barsoum, M. Radovic, Elastic and mechanical properties of the MAX phases, Annu. Rev. Mater. Res. 41 (2011) 195–227.
[20] M. Magnuson, M. Mattesini, Chemical bonding and electronic-structure in MAX phases as viewed by X-ray spectroscopy and density functional theory, Thin Solid Films 621 (2017) 108–130.
[21] X. Xie, S. Chen, W. Ding, Y. Nie, Z. Wei, An extraordinarily stable catalyst: Pt NPs supported on two-dimensional $Ti_3C_2X_2$ (X = OH, F) nanosheets for oxygen reduction reaction, Chem. Commun. 49 (2013) 10112–10114.
[22] M. Han, X. Yin, H. Wu, Z. Hou, C. Song, X. Li, L. Zhang, L. Cheng, Ti_3C_2MXenes with Modified Surface for High-Performance Electromagnetic Absorption and Shielding in the X-Band, ACS Appl. Mater. Interfaces 8 (2016) 21011–21019.
[23] J. Liu, Y. Liu, N. Liu, Y. Han, X. Zhang, H. Huang, Y. Lifshitz, S.T. Lee, J. Zhong, Z. Kang, Metal-free efficient photocatalyst for stable visible water splitting via a two-electron pathway, Science. 347 (2015) 970–974.
[24] T.Y. Ma, J.L. Cao, M. Jaroniec, S.Z. Qiao, Interacting carbon nitride and titanium carbide nanosheets for high-performance oxygen evolution, Angew. Chemie Int. Ed. 55 (2016) 1138–1142.
[25] X. Zhang, X. Zhao, D. Wu, Y. Jing, Z. Zhou, High and anisotropic carrier mobility in experimentally possible Ti_2CO_2 (MXene) monolayers and nanoribbons, Nanoscale 7 (2015) 16020–16025.

[26] R. Wu, H. Du, Z. Wang, M. Gao, H. Pan, Y. Liu, Remarkably improved hydrogen storage properties of $NaAlH_4$ doped with 2D titanium carbide, J. Power Sources 327 (2016) 519–525.
[27] G. Zou, B. Liu, J. Guo, Q. Zhang, C. Fernandez, Q. Peng, Synthesis of nanoflower-shaped MXene derivative with unexpected catalytic activity for dehydrogenation of sodium alanates, ACS Appl. Mater. Interfaces 9 (2017) 7611–7618.
[28] J. Ran, G. Gao, F.T. Li, T.-Y. Ma, A. Du, S.Z. Qiao, Ti_3C_2 MXene co-catalyst on metal sulfide photo-absorbers for enhanced visible-light photocatalytic hydrogen production, Nat. Commun. 8 (2017) 13907.
[29] Z. Guo, J. Zhou, L. Zhu, Z. Sun, MXene: a promising photocatalyst for water splitting, J. Mater. Chem. A 4 (2016) 11446–11452.
[30] H. Liu, C. Duan, C. Yang, W. Shen, F. Wang, Z. Zhu, A novel nitrite biosensor based on the direct electrochemistry of hemoglobin immobilized on MXene-Ti_3C_2, Sens. Actuators B Chem. 218 (2015) 60–66.
[31] X.F. Yu, Y.C. Li, J.B. Cheng, Z.B. Liu, Q.Z. Li, W.-Z. Li, X. Yang, B. Xiao, Monolayer Ti_2CO_2: a promising candidate for NH_3 sensor or capturer with high sensitivity and selectivity, ACS Appl. Mater. Interfaces 7 (2015) 13707–13713.
[32] Q. Xue, H. Zhang, M. Zhu, Z. Pei, H. Li, Z. Wang, Y. Huang, Y. Huang, Q. Deng, J. Zhou, S. Du, Q. Huang, C. Zhi, Photoluminescent Ti_3C_2 MXene quantum dots for multicolor cellular imaging, Adv. Mater. 29 (2017), 1604847.
[33] J.W. Park, D.Y. Lee, H. Kim, J.S. Hyeon, M.J. de Andrade, R.H. Baughman, S.J. Kim, Highly loaded MXene/carbon nanotube yarn electrodes for improved asymmetric supercapacitor performance, MRS Commun. 9 (2019) 114–121.
[34] M. Naguib, J. Come, B. Dyatkin, V. Presser, P.-L. Taberna, P. Simon, M.W. Barsoum, Y. Gogotsi, MXene: a promising transition metal carbide anode for lithium-ion batteries, Electrochem. Commun. 16 (2012) 61–64.
[35] X. Wang, S. Kajiyama, H. Iinuma, E. Hosono, S. Oro, I. Moriguchi, M. Okubo, A. Yamada, Pseudocapacitance of MXene nanosheets for high-power sodium-ion hybrid capacitors, Nat. Comm. 6 (2015) 6544.
[36] X. Xie, M.-Q. Zhao, B. Anasori, K. Maleski, C.E. Ren, J. Li, B.W. Byles, E. Pomerantseva, G. Wang, Y. Gogotsi, Porous heterostructured MXene/carbon nanotube composite paper with high volumetric capacity for sodium-based energy storage devices, Nano Energy 26 (2016) 513–523.
[37] M. Hu, T. Hu, R. Cheng, J. Yang, C. Cui, C. Zhang, X. Wang, MXene-coated silk-derived carbon cloth toward flexible electrode for supercapacitor application, J. Energy Chem. 27 (2018) 161–166.
[38] Z. Li, L. Wang, D. Sun, Y. Zhang, B. Liu, Q. Hu, A. Zhou, Synthesis and thermal stability of two-dimensional carbide MXene Ti_3C_2, Mater. Sci. Eng. B 191 (2015) 33–40.
[39] A. VahidMohammadi, A. Hadjikhani, S. Shahbazmohamadi, M. Beidaghi, Two-dimensional vanadium carbide (MXene) as a high-capacity cathode material for rechargeable aluminum batteries, ACS Nano 11 (2017) 11135–11144.
[40] L.M. Viculis, J.J. Mack, O.M. Mayer, H.T. Hahn, R.B. Kaner, Intercalation and exfoliation routes to graphite nanoplatelets, J. Mater. Chem. 15 (2005) 974–978.
[41] M. Naguib, O. Mashtalir, J. Carle, V. Presser, J. Lu, L. Hultman, Y. Gogotsi, M.W. Barsoum, Two-dimensional transition metal carbides, ACS Nano 6 (2012) 1322–1331.
[42] N.K. Chaudhari, H. Jin, B. Kim, D. San Baek, S.H. Joo, K. Lee, MXene: an emerging two-dimensional material for future energy conversion and storage applications, J. Mater. Chem. A 5 (2017) 24564–24579.
[43] F. Chang, C. Li, J. Yang, H. Tang, M. Xue, Synthesis of a new graphene-like transition metal carbide by de-intercalating Ti_3AlC_2, Mater. Lett. 109 (2013) 295–298.
[44] Z. Sun, S. Li, R. Ahuja, J.M. Schneider, Calculated elastic properties of M_2AlC (M=Ti, V, Cr, Nb and Ta), Solid State Commun. 129 (2004) 589–592.
[45] M. Alhabeb, K. Maleski, B. Anasori, P. Lelyukh, L. Clark, S. Sin, Y. Gogotsi, Guidelines for Synthesis and Processing of Two-Dimensional Titanium Carbide ($Ti_3C_2T_x$ MXene), Chem. Mater. 29 (2017) 7633–7644.
[46] J. Halim, M.R. Lukatskaya, K.M. Cook, J. Lu, C.R. Smith, L.-Å. Näslund, S.J. May, L. Hultman, Y. Gogotsi, P. Eklund, M.W. Barsoum, Transparent conductive two-dimensional titanium carbide epitaxial thin films, Chem. Mater. 26 (2014) 2374–2381.
[47] C. Shen, L. Wang, A. Zhou, B. Wang, X. Wang, W. Lian, Q. Hu, G. Qin, X. Liu, Synthesis and electrochemical properties of two-dimensional RGO/Ti3C2T(x) nanocomposites, Nanomaterials (Basel, Switzerland). 8 (2018) 80.
[48] F. Liu, A. Zhou, J. Chen, J. Jia, W. Zhou, L. Wang, Q. Hu, Preparation of Ti_3C_2 and Ti_2C MXenes by fluoride salts etching and methane adsorptive properties, Appl. Surf. Sci. 416 (2017) 781–789.
[49] M.R. Lukatskaya, O. Mashtalir, C.E. Ren, Y. Dall'Agnese, P. Rozier, P.L. Taberna, M. Naguib, P. Simon, M.W. Barsoum, Y. Gogotsi, Cation intercalation and high volumetric capacitance of two-dimensional titanium carbide, Science. 341 (2013) 1502–1505.
[50] M. Ghidiu, M.R. Lukatskaya, M.Q. Zhao, Y. Gogotsi, M.W. Barsoum, Conductive two-dimensional titanium carbide 'clay' with high volumetric capacitance, Nature. 516 (2014) 78.
[51] I.R. Shein, A.L. Ivanovskii, Graphene-like titanium carbides and nitrides $Ti_{n+1}C_n$, $Ti_{n+1}N_n$ (n=1, 2, and 3) from de-intercalated MAX phases: first-principles probing of their structural, electronic properties and relative stability, Comput. Mater. Sci. 65 (2012) 104–114.
[52] P. Urbankowski, B. Anasori, T. Makaryan, D. Er, S. Kota, P.L. Walsh, M. Zhao, V.B. Shenoy, M.W. Barsoum, Y. Gogotsi, Synthesis of two-dimensional titanium nitride Ti_4N_3 (MXene), Nanoscale. 8 (2016) 11385–11391.
[53] B. Soundiraraju, B.K. George, Two-dimensional titanium nitride (Ti_2N) MXene: synthesis, characterization, and potential application as surface-enhanced raman scattering substrate, ACS Nano 11 (2017) 8892–8900.
[54] A. Djire, A. Bos, J. Liu, H. Zhang, E.M. Miller, N.R. Neale, Pseudocapacitive Storage in Nanolayered Ti2NTx MXene Using Mg-Ion Electrolyte, ACS Appl. Nano Mater. 2 (2019) 2785–2795.
[55] A. Djire, H. Zhang, J. Liu, E.M. Miller, N.R. Neale, Electrocatalytic and optoelectronic characteristics of the two-dimensional titanium nitride $Ti_4N_3T_x$ MXene, ACS Appl. Mater. Interfaces 11 (2019) 11812–11823.
[56] O. Mashtalir, M. Naguib, V.N. Mochalin, Y. Dall'Agnese, M. Heon, M.W. Barsoum, Y. Gogotsi, Intercalation and delamination of layered carbides and carbonitrides, Nat. Comm. 4 (2013) 1716.
[57] M. Naguib, R.R. Unocic, B.L. Armstrong, J. Nanda, Large-scale delamination of multi-layers transition metal carbides and carbonitrides "MXenes", Dalton Trans. 44 (2015) 9353–9358.
[58] K. Rasool, M. Helal, A. Ali, C.E. Ren, Y. Gogotsi, K.A. Mahmoud, Antibacterial activity of $Ti_3C_2T_x$ MXene, ACS Nano 10 (2016) 3674–3684.
[59] B. Xu, M. Zhu, W. Zhang, X. Zhen, Z. Pei, Q. Xue, C. Zhi, P. Shi, Ultrathin MXene-Micropattern-Based field-effect transistor for probing neural activity, Adv. Mater. 28 (2016) 3333–3339.
[60] K.D. Fredrickson, B. Anasori, Z.W. Seh, Y. Gogotsi, A. Vojvodic, Effects of applied potential and water intercalation on the surface chemistry of Ti_2C and Mo_2C MXenes, J. Phys. Chem. C 120 (2016) 28432–28440.
[61] Q. Yang, Z. Xu, B. Fang, T. Huang, S. Cai, H. Chen, Y. Liu, K. Gopalsamy, W. Gao, C. Gao, MXene/graphene hybrid fibers for high performance flexible supercapacitors, J. Mater. Chem. A 5 (2017) 22113–22119.
[62] F. Liu, J. Zhou, S. Wang, B. Wang, C. Shen, L. Wang, Q. Hu, Q. Huang, A. Zhou, Preparation of high-purity V_2C MXene and electrochemical properties as Li-Ion batteries, J. Electrochem. Soc. 164 (2017) A709–A713.
[63] J. Zhou, X. Zha, X. Zhou, F. Chen, G. Gao, S. Wang, C. Shen, T. Chen, C. Zhi, P. Eklund, S. Du, J. Xue, W. Shi, Z. Chai, Q. Huang, Synthesis and electrochemical properties of two-dimensional hafnium carbide, ACS Nano 11 (2017) 3841–3850.
[64] O. Mashtalir, M.R. Lukatskaya, M.-Q. Zhao, M.W. Barsoum, Y. Gogotsi, Amine-assisted delamination of Nb_2C MXene for Li-Ion energy storage devices, Adv. Mater. 27 (2015) 3501–3506.
[65] B. Anasori, Y. Xie, M. Beidaghi, J. Lu, B.C. Hosler, L. Hultman, P.R.C. Kent, Y. Gogotsi, M.W. Barsoum, Two-Dimensional, Ordered, Double Transition Metals Carbides (MXenes), ACS Nano 9 (2015) 9507–9516.
[66] L. Wang, H. Zhang, B. Wang, C. Shen, C. Zhang, Q. Hu, A. Zhou, B. Liu, Synthesis and electrochemical performance of $Ti_3C_2T_x$ with hydrothermal process, Electron. Mater. Lett. 12 (2016) 702–710.
[67] O. Mashtalir, M. Lukatskaya, A. Kolesnikov, E. Raymundo-Pin˜ero, M. Naguib, M. Barsoum, Y. Gogotsi, Effect of hydrazine intercalation on structure and capacitance of 2D titanium carbide (MXene), Nanoscale. 8 (2016).
[68] Y. Yoon, T.A. Le, A.P. Tiwari, I. Kim, M.W. Barsoum, H. Lee, Low temperature solution synthesis of reduced two dimensional Ti_3C_2 MXenes with paramagnetic behaviour, Nanoscale 10 (2018) 22429–22438.
[69] Y. Wang, H. Dou, J. Wang, B. Ding, Y. Xu, Z. Chang, X. Hao, Three-dimensional porous MXene/layered double hydroxide composite for high performance supercapacitors, J. Power Sources 327 (2016) 221–228.
[70] S. Xu, G. Wei, J. Li, Y. Ji, N. Klyui, V. Izotov, W. Han, Binder-free $Ti_3C_2T_x$ MXene electrode film for supercapacitor produced by electrophoretic deposition method, Chem. Eng. J. 317 (2017) 1026–1036.
[71] A.S. Levitt, M. Alhabeb, C.B. Hatter, A. Sarycheva, G. Dion, Y. Gogotsi, Electrospun MXene/carbon nanofibers as supercapacitor electrodes, J. Mater. Chem. A 7 (2019) 269–277.
[72] X. Wang, S. Lin, H. Tong, Y. Huang, P. Tong, B. Zhao, J. Dai, C. Liang, H. Wang, X. Zhu, Y. Sun, S. Dou, Two-dimensional V_4C_3 MXene as high performance electrode materials for supercapacitors, Electrochim. Acta 307 (2019) 414–421.
[73] K. Maleski, V.N. Mochalin, Y. Gogotsi, Dispersions of two-dimensional titanium carbide MXene in organic solvents, Chem. Mater. 29 (2017) 1632–1640.
[74] J. Xuan, Z. Wang, Y. Chen, D. Liang, L. Cheng, X. Yang, Z. Liu, R. Ma, T. Sasaki, F. Geng, Organic-Base-Driven Intercalation and Delamination for the Production of Functionalized Titanium Carbide Nanosheets with Superior Photothermal Therapeutic Performance, Angew. Chemie Int. Ed. 55 (2016) 14569–14574.
[75] Y. Wu, P. Nie, J. Wang, H. Dou, X. Zhang, Few-layer MXenes delaminated via high-energy mechanical milling for enhanced sodium-ion batteries performance, ACS Appl. Mater. Interfaces 9 (2017) 39610–39617.
[76] M. Khazaei, A. Ranjbar, M. Arai, T. Sasaki, S. Yunoki, Electronic properties and applications of MXenes: a theoretical review, J. Mater. Chem. C 5 (2017) 2488–2503.
[77] M. Ashton, K. Mathew, R.G. Hennig, S.B. Sinnott, Predicted surface composition and thermodynamic stability of MXenes in solution, J. Phys. Chem. C 120 (2016) 3550–3556.
[78] P.O.Å. Persson, in: B. Anasori, Y. Gogotsi (Eds.), MXene Surface Chemistry, in 2D Metal Carbides and Nitrides (MXenes): Structure, Properties and Applications, Springer International Publishing, Cham, 2019, pp. 125–136.

[79] M.A. Hope, A.C. Forse, K.J. Griffith, M.R. Lukatskaya, M. Ghidiu, Y. Gogotsi, C.P. Grey, NMR reveals the surface functionalisation of Ti_3C_2 MXene, Phys. Chem. Chem. Phys. 18 (2016) 5099–5102.
[80] Y. Liu, H. Xiao, W.A. Goddard, Schottky-barrier-Free contacts with two-dimensional semiconductors by surface-engineered MXenes, J. Am. Chem. Soc. 138 (2016) 15853–15856.
[81] Y. Zhong, X. Xia, F. Shi, J. Zhan, J. Tu, H.J. Fan, Transition metal carbides and nitrides in energy storage and conversion, Adv. Sci. 3 (2016), 1500286.
[82] O. Mashtalir, K.M. Cook, V.N. Mochalin, M. Crowe, M.W. Barsoum, Y. Gogotsi, Dye adsorption and decomposition on two-dimensional titanium carbide in aqueous media, J. Mater. Chem. A 2 (2014) 14334–14338.
[83] C.J. Zhang, S. Pinilla, N. McEvoy, C.P. Cullen, B. Anasori, E. Long, S.H. Park, A. Seral-Ascaso, A. Shmeliov, D. Krishnan, C. Morant, X. Liu, G.S. Duesberg, Y. Gogotsi, V. Nicolosi, Oxidation stability of colloidal two-dimensional titanium carbides (MXenes), Chem. Mater. 29 (2017) 4848–4856.
[84] Z. Ling, C.E. Ren, M.-Q. Zhao, J. Yang, J.M. Giammarco, J. Qiu, M.W. Barsoum, Y. Gogotsi, Flexible and conductive MXene films and nanocomposites with high capacitance, Proc. Natl. Acad. Sci. 111 (2014) 16676–16681.
[85] K. Hantanasirisakul, M.-Q. Zhao, P. Urbankowski, J. Halim, B. Anasori, S. Kota, C.E. Ren, M.W. Barsoum, Y. Gogotsi, Fabrication of $Ti_3C_2T_x$ MXene transparent thin films with tunable optoelectronic properties, Adv. Electron. Mater. 2 (2016), 1600050.
[86] A.D. Dillon, M.J. Ghidiu, A.L. Krick, J. Griggs, S.J. May, Y. Gogotsi, M.W. Barsoum, A.T. Fafarman, Highly conductive optical quality solution-processed films of 2D titanium carbide, Adv. Funct. Mater. 26 (2016) 4162–4168.
[87] M. Khazaei, M. Arai, T. Sasaki, C.-Y. Chung, N.S. Venkataramanan, M. Estili, Y. Sakka, Y. Kawazoe, Novel electronic and magnetic properties of two-dimensional transition metal carbides and nitrides, Adv. Funct. Mater. 23 (2013) 2185–2192.
[88] J. Yang, M. Naguib, M. Ghidiu, L.-M. Pan, J. Gu, J. Nanda, J. Halim, Y. Gogotsi, M.W. Barsoum, Two-dimensional Nb-Based M_4C_3 solid solutions (MXenes), J. Am. Ceram. Soc. 99 (2016) 660–666.
[89] M. Naguib, J. Halim, J. Lu, K.M. Cook, L. Hultman, Y. Gogotsi, M.W. Barsoum, New two-dimensional niobium and vanadium carbides as promising materials for Li-Ion batteries, J. Am. Chem. Soc. 135 (2013) 15966–15969.
[90] R. Meshkian, Q. Tao, M. Dahlqvist, J. Lu, L. Hultman, J. Rosen, Theoretical stability and materials synthesis of a chemically ordered MAX phase, Mo_2ScAlC_2, and its two-dimensional derivate Mo_2ScC_2 MXene, Acta Mater. 125 (2017) 476–480.
[91] Z.W. Seh, K.D. Fredrickson, B. Anasori, J. Kibsgaard, A.L. Strickler, M.R. Lukatskaya, Y. Gogotsi, T.F. Jaramillo, A. Vojvodic, Two-dimensional molybdenum carbide (MXene) as an efficient electrocatalyst for hydrogen evolution, ACS Energy Lett. 1 (2016) 589–594.
[92] J. Zhou, X. Zha, F.Y. Chen, Q. Ye, P. Eklund, S. Du, Q. Huang, A two-dimensional zirconium carbide by selective etching of Al3C3 from nanolaminated Zr3Al3C5, Angew. Chemie Int. Ed. 55 (2016) 5008–5013.
[93] P. Urbankowski, B. Anasori, K. Hantanasirisakul, L. Yang, L. Zhang, B. Haines, S.J. May, S.J.L. Billinge, Y. Gogotsi, 2D molybdenum and vanadium nitrides synthesized by ammoniation of 2D transition metal carbides (MXenes), Nanoscale. 9 (2017) 17722–17730.
[94] D. Sun, M. Wang, Z. Li, G. Fan, L.-Z. Fan, A. Zhou, Two-dimensional Ti_3C_2 as anode material for Li-ion batteries, Electrochem. Commun. 47 (2014) 80–83.
[95] S.J. Kim, M. Naguib, M. Zhao, C. Zhang, H.-T. Jung, M.W. Barsoum, Y. Gogotsi, High mass loading, binder-free MXene anodes for high areal capacity Li-ion batteries, Electrochim. Acta 163 (2015) 246–251.
[96] C. Chen, X. Xie, B. Anasori, A. Sarycheva, T. Makaryan, M. Zhao, P. Urbankowski, L. Miao, J. Jiang, Y. Gogotsi, MoS_2-on-MXene heterostructures as highly reversible anode materials for lithium-ion batteries, Angew. Chemie Int. Ed. 57 (2018) 1846–1850.
[97] Z. Ma, X. Zhou, W. Deng, D. Lei, Z. Liu, 3D porous MXene (Ti_3C_2)/Reduced graphene oxide hybrid films for advanced Lithium storage, ACS Appl. Mater. Interfaces 10 (2018) 3634–3643.
[98] Y. Wang, Y. Li, Z. Qiu, X. Wu, P. Zhou, T. Zhou, J. Zhao, Z. Miao, J. Zhou, S. Zhuo, Fe_3O_4@Ti_3C_2 MXene hybrids with ultrahigh volumetric capacity as an anode material for lithium-ion batteries, J. Mater. Chem. A 6 (2018) 11189–11197.
[99] J. Zhu, A. Chroneos, J. Eppinger, U. Schwingenschlögl, S-functionalized MXenes as electrode materials for Li-ion batteries, Appl. Mater. Today. 5 (2016) 19–24.
[100] Q. Meng, J. Ma, Y. Zhang, Z. Li, A. Hu, J.-J. Kai, J. Fan, Theoretical investigation of zirconium carbide MXenes as prospective high capacity anode materials for Na-ion batteries, J. Mater. Chem. A 6 (2018) 13652–13660.
[101] Y. Xie, Y. Dall'Agnese, M. Naguib, Y. Gogotsi, M.W. Barsoum, H.L. Zhuang, P.R.C. Kent, Prediction and characterization of MXene nanosheet anodes for non-lithium-Ion batteries, ACS Nano 8 (2014) 9606–9615.
[102] Q. Tang, Z. Zhou, P. Shen, Are MXenes promising anode materials for Li Ion Batteries? Computational studies on electronic properties and Li storage capability of Ti_3C_2 and $Ti_3C_2X_2$ (X = F, OH) monolayer, J. Am. Chem. Soc. 134 (2012) 16909–16916.
[103] M.R. Lukatskaya, S.-M. Bak, X. Yu, X.Q. Yang, M.W. Barsoum, Y. Gogotsi, Probing the mechanism of high capacitance in 2D titanium carbide using in situ X-Ray absorption spectroscopy, Adv. Energy Mater. 5 (2015), 1500589.
[104] M. Hu, Z. Li, T. Hu, S. Zhu, C. Zhang, X. Wang, High-capacitance mechanism for $Ti_3C_2T_x$ MXene by in situ electrochemical raman spectroscopy investigation, ACS Nano 10 (2016) 11344–11350.
[105] L. Li, N. Zhang, M. Zhang, L. Wu, X. Zhang, Z. Zhang, Ag-nanoparticle-Decorated 2D titanium carbide (MXene) with superior electrochemical performance for supercapacitors, ACS Sustain. Chem. Eng. 6 (2018) 7442–7450.
[106] J. Li, X. Yuan, C. Lin, Y. Yang, L. Xu, X. Du, J. Xie, J. Lin, J. Sun, Achieving high pseudocapacitance of 2D titanium carbide (MXene) by cation intercalation and surface modification, Adv. Energy Mater. 7 (2017), 1602725.
[107] X. Zhang, Z. Zhang, Z. Zhou, MXene-based materials for electrochemical energy storage, J. Energy Chem. 27 (2018) 73–85.
[108] B. Anasori, M.R. Lukatskaya, Y. Gogotsi, 2D metal carbides and nitrides (MXenes) for energy storage, Nat. Rev. Mater. 2 (2017) 16098.
[109] C. Zhang, V. Nicolosi, Graphene and MXene-based transparent conductive electrodes and supercapacitors, Energy Storage Mater. 16 (2019) 102–125.
[110] Y. Dall'Agnese, M.R. Lukatskaya, K.M. Cook, P.L. Taberna, Y. Gogotsi, P. Simon, High capacitance of surface-modified 2D titanium carbide in acidic electrolyte, Electrochem. Commun. 48 (2014) 118–122.
[111] X. An, W. Wang, J. Wang, H. Duan, J. Shi, X. Yu, The synergetic effects of Ti_3C_2 MXene and Pt as co-catalysts for highly efficient photocatalytic hydrogen evolution over g-C3N4, Phys. Chem. Chem. Phys. 20 (2018) 11405–11411.
[112] M. Zhu, Y. Huang, Q. Deng, J. Zhou, Z. Pei, Q. Xue, Y. Huang, Z. Wang, H. Li, Q. Huang, C. Zhi, Highly flexible, freestanding supercapacitor electrode with enhanced performance obtained by hybridizing polypyrrole chains with MXene, Adv. Energy Mater. 6 (2016), 1600969.
[113] Y. Wen, T.E. Rufford, X. Chen, N. Li, M. Lyu, L. Dai, L. Wang, Nitrogen-doped Ti3C2Tx MXene electrodes for high-performance supercapacitors, Nano Energy 38 (2017) 368–376.
[114] G. Gao, A.P. O'Mullane, A. Du, 2D MXenes: a new family of promising catalysts for the hydrogen evolution reaction, ACS Catal. 7 (2017) 494–500.
[115] H. Pan, Ultra-high electrochemical catalytic activity of MXenes, Sci. Rep. 6 (2016) 32531.
[116] M. Pandey, K.S. Thygesen, Two-dimensional MXenes as catalysts for electrochemical hydrogen evolution: a computational screening study, J. Phys. Chem. C 121 (2017) 13593–13598.
[117] X. Zhang, Z. Zhang, J. Li, X. Zhao, D. Wu, Z. Zhou, Ti_2CO_2 MXene: a highly active and selective photocatalyst for CO2 reduction, J. Mater. Chem. A 5 (2017) 12899–12903.
[118] J. Zhu, E. Ha, G. Zhao, Y. Zhou, D. Huang, G. Yue, L. Hu, N. Sun, Y. Wang, L.Y.S. Lee, C. Xu, K.-Y. Wong, D. Astruc, P. Zhao, Recent advance in MXenes: a promising 2D material for catalysis, sensor and chemical adsorption, Coord. Chem. Rev. 352 (2017) 306–327.
[119] S.J. Kim, H.-J. Koh, C.E. Ren, O. Kwon, K. Maleski, S.-Y. Cho, B. Anasori, C.-K. Kim, Y.-K. Choi, J. Kim, Y. Gogotsi, H.-T. Jung, Metallic $Ti_3C_2T_x$ MXene gas sensors with ultrahigh signal-to-Noise ratio, ACS Nano 12 (2018) 986–993.
[120] R.B. Rakhi, P. Nayak, C. Xia, H.N. Alshareef, Novel amperometric glucose biosensor based on MXene nanocomposite, Sci. Rep. 6 (2016) 36422.
[121] Y. Ma, N. Liu, L. Li, X. Hu, Z. Zou, J. Wang, S. Luo, Y. Gao, A highly flexible and sensitive piezoresistive sensor based on MXene with greatly changed interlayer distances, Nat. Commun. 8 (2017) 1207.
[122] G. Zou, J. Guo, Q. Peng, A. Zhou, Q. Zhang, B. Liu, Synthesis of urchin-like rutile titania carbon nanocomposites by iron-facilitated phase transformation of MXene for environmental remediation, J. Mater. Chem. A 4 (2016) 489–499.
[123] A. Shahzad, K. Rasool, W. Miran, M. Nawaz, J. Jang, K.A. Mahmoud, D.S. Lee, Two-dimensional $Ti_3C_2T_x$ MXene nanosheets for efficient copper removal from water, ACS Sustain. Chem. Eng. 5 (2017) 11481–11488.
[124] Q. Peng, J. Guo, Q. Zhang, J. Xiang, B. Liu, A. Zhou, R. Liu, Y. Tian, Unique lead adsorption behavior of activated hydroxyl group in two-dimensional titanium carbide, J. Am. Chem. Soc. 136 (2014) 4113–4116.
[125] Q. Zhang, J. Teng, G. Zou, Q. Peng, Q. Du, T. Jiao, J. Xiang, Efficient phosphate sequestration for water purification by unique sandwich-like MXene/magnetic iron oxide nanocomposites, Nanoscale 8 (2016) 7085–7093.
[126] Y.-J. Zhang, J.-H. Lan, L. Wang, Q.-Y. Wu, C.-Z. Wang, T. Bo, Z.-F. Chai, W.-Q. Shi, Adsorption of uranyl species on hydroxylated titanium carbide nanosheet: a first-principles study, J. Hazard. Mater. 308 (2016) 402–410.
[127] J. Guo, Q. Peng, H. Fu, G. Zou, Q. Zhang, Heavy-metal adsorption behavior of two-dimensional alkalization-intercalated MXene by first-principles calculations, J. Phys. Chem. C 119 (2015) 20923–20930.
[128] F. Shahzad, M. Alhabeb, C.B. Hatter, B. Anasori, S. Man Hong, C.M. Koo, Y. Gogotsi, Electromagnetic interference shielding with 2D transition metal carbides (MXenes), Science 353 (2016) 1137–1140.
[129] Y. Qing, W. Zhou, F. Luo, D. Zhu, Titanium carbide (MXene) nanosheets as promising microwave absorbers, Ceram. Int. 42 (2016) 16412–16416.
[130] J. Liu, H.-B. Zhang, R. Sun, Y. Liu, Z. Liu, A. Zhou, Z.-Z. Yu, Hydrophobic, Flexible, and Lightweight MXene Foams for High-Performance Electromagnetic-Interference Shielding, Adv. Mater. 29 (2017), 1702367.
[131] X. Zhang, M. Xue, X. Yang, Z. Wang, G. Luo, Z. Huang, X. Sui, C. Li, Preparation and tribological properties of $Ti_3C_2(OH)_2$ nanosheets as additives in base oil, RSC Adv. 5 (2015) 2762–2767.
[132] G. Ying, S. Kota, A.D. Dillon, A.T. Fafarman, M.W. Barsoum, Conductive transparent V_2CT_x (MXene) films, FlatChem. 8 (2018) 25–30.
[133] A. Ali, A. Belaidi, S. Ali, M.I. Helal, K. Mahmoud, Transparent and Conductive $Ti_3C_2T_x$ (MXene) Thin Film Fabrication by Electrohydrodynamic Atomization Technique, Vol. 27, 2016.

[134] K. Rasool, K.A. Mahmoud, D.J. Johnson, M. Helal, G.R. Berdiyorov, Y. Gogotsi, Efficient antibacterial membrane based on two-dimensional Ti(3)C(2)T(x) (MXene) nanosheets, Sci. Rep. 7 (2017), 1598-1598.
[135] A. Jastrzębska, E. Karwowska, T. Wojciechowski, W. Ziemkowska, A. Wojciechowska, L. Chlubny, A. Olszyna, The Atomic Structure of Ti_2C and Ti_3C_2 MXenes Is Responsible for Their Antibacterial Activity Toward E. Coli Bacteria, 2018.
[136] C.L. Manzanares-Palenzuela, A.M. Pourrahimi, J. Gonzalez-Julian, Z. Sofer, M. Pykal, M. Otyepka, M. Pumera, Interaction of single- and double-stranded DNA with multilayer MXene by fluorescence spectroscopy and molecular dynamics simulations, Chem. Sci. (2019).
[137] N.F. Rosli, M.Z.M. Nasir, N. Antonatos, Z. Sofer, A. Dash, J. Gonzalez-Julian, A.C. Fisher, R.D. Webster, M. Pumera, MAX and MAB Phases: Two-Dimensional Layered Carbide and Boride Nanomaterials for Electrochemical Applications, ACS Appl. Nano Mater. 2 (2019) 6010–6021.
[138] Z. Ma, Z. Hu, X. Zhao, Q. Tang, D. Wu, Z. Zhou, L. Zhang, Tunable band structures of heterostructured bilayers with transition-metal dichalcogenide and MXene monolayer, J. Phys. Chem. C 118 (2014) 5593–5599.
[139] J. Xu, J. Shim, J.-H. Park, S. Lee, MXene electrode for the integration of WSe_2 and MoS_2 field effect transistors, Adv. Funct. Mater. 26 (2016) 5328–5334.
[140] J. Vyskočil, C.C. Mayorga-Martinez, K. Szőkölová, A. Dash, J. Gonzalez-Julian, Z. Sofer, M. Pumera, 2D stacks of MXene Ti_3C_2 and 1T-Phase $WS_2$with enhanced capacitive behavior, Chem. Electro. Chem. 6 (2019) 3982.